AERODYNAMIC ANALYSIS OF FLATBACK AIRFOILS USING VORTEX PARTICLE METHOD

A THESIS SUBMITTED TO
THE GRADUATE SCHOOL OF NATURAL AND APPLIED SCIENCES
OF
MIDDLE EAST TECHNICAL UNIVERSITY

BY

SENEM AYŞE HASER

IN PARTIAL FULFILLMENT OF THE REQUIREMENTS
FOR
THE DEGREE OF MASTER OF SCIENCE
IN
AEROSPACE ENGINEERING

DECEMBER 2014

Approval of the thesis:

AERODYNAMIC ANALYSIS OF FLATBACK AIRFOILS USING VORTEX PARTICLE METHOD

submitted by **SENEM AYŞE HASER** in partial fulfillment of the requirements for the degree of **Master of Sciencein Aerospace Engineering Department, Middle East Technical University** by,

Prof. Dr. Gülbin Dural Ünver _____
Dean, Graduate School of **Natural and Applied Sciences**

Prof. Dr. Ozan Tekinalp _____
Head of Department, **Aerospace Engineering**

Assoc. Prof. Dr. Oğuz Uzol _____
Supervisor, **Aerospace Engineering Dept., METU**

Examining Committee Members:

Prof. Dr. İsmail Hakkı Tuncer _____
Aerospace Engineering Dept., METU

Assoc. Prof. Dr. Oğuz Uzol _____
Aerospace Engineering Dept., METU

Assoc. Prof. Dr. Dilek Funda Kurtuluş Bozdemir _____
Aerospace Engineering Dept., METU

Assoc. Prof. Dr. Sinan Eyi _____
Aerospace Engineering Dept., METU

Assoc. Prof. Dr. Özgür Kurç _____
Civil Engineering Dept., METU

Date: 05.12.2014

I hereby declare that all information in this document has been obtained and presented in accordance with academic rules and ethical conduct. I also declare that, as required by these rules and conduct, I have fully cited and referenced all material and results that are not original to this work.

Name, Last Name: Senem Ayşe Haser

Signature:

ABSTRACT

AERODYNAMIC ANALYSIS OF FLATBACK AIRFOILS USING VORTEX PARTICLE METHOD

Haser, Senem Ayşe
MS., Department of Aerospace Engineering
Supervisor: Assoc. Prof. Dr. Oğuz Uzol

December 2014, 70 pages

In this thesis, aerodynamic analysis of flatback airfoils, which have been proposed and investigated to improve the aerodynamic performance of thick airfoils, is studied. Vortex particle method, which is commonly used for simulation of two dimensional, incompressible, viscous flows, is used for this purpose. In the content of this thesis, vortex particle method code developed by Kaya [1] is improved by changing method of diffusion and method of vorticity releasing from solid boundary. Deterministic Particle Strength Exchange (PSE) method is implemented to solve diffusion equation. In addition, instead of vortex particle releasing algorithm, vorticity releasing algorithm, which is more suitable for PSE method, is implemented.

The method and algorithm are explained in detail and results of analysis are presented. The validation and applicability of the improved code is illustrated by solving flow past a flat plate, a circular cylinder and a square cylinder. After that, flow around FB3500 series flatback airfoils at Reynolds number of 1000 are simulated by using the improved vortex particle method code. In order to compare

results, laminar and unsteady Computational Fluid Dynamics (CFD) analyses are performed.

Keywords: Vortex Particle Method, Particle Strength Exchange, Flatback Airfoil

ÖZ

KÜT FİRAR KENARLI KANAT KESİTLERİNİN GİRDAP PARÇACIK YÖNTEMİ İLE AERODİNAMİK ANALİZİ

Haser, Senem Ayşe
Yüksek Lisans, Havacılık ve Uzay Mühendisliği Bölümü
Tez Yöneticisi: Doç. Dr. Oğuz Uzol

Aralık 2014, 70 sayfa

Bu tezde, kalın profillerin performansını arttırmak için önerilen ve son zamanlarda sıklıkla araştırılan bir konu olan küt firar kenarlı kanat kesitlerinin aerodinamik analizleri anlatılmaktadır. Analizler, küt cisimler etrafından geçen iki boyutlu, sıkıştırılamayan, sürtünmeli akımların simulasyonlarında sıklıkla kullanılan girdap parçacık yöntemi ile gerçekleştirilmiştir. Bu tezin kapsamında, Kaya [1] tarafından geliştirilen girdap parçacık yöntemi kodu, difüzyon ve model sınırlarından akışa girdap gücü salınımı yöntemleri değiştirilerek geliştirilmiştir. Difüzyon yöntemi olarak deterministik bir yöntem olan Parçacık Gücü Değişimi (PGD) yöntemi kullanılmıştır. Ayrıca, sınırda oluşan girdap parçacıklarını akışa bırakma yöntemi yerine, parçacıkların girdap güçlerini akışa salınımı yöntemi uygulanmıştır. Bu yöntem, PGD difüzyon yöntemi için daha uygun bir yöntemdir.

Tezde, kullanılan yöntem ve geliştirilen algoritmanın detayları ve analiz sonuçları anlatılmaktadır. Geliştirilen algotitmanın doğruluğu ve uygulanabilirliği düz plaka, kare kesitli silindir ve dairesel kesitli silindir etrafındaki akış çözümlenerek gösterilmiştir. Sonrasında, FB3500 serisi küt firar kenarlı kanat kesitleri etrafındaki

1000 Reynolds sayısındaki akış alanı çözülmüştür. Sonuçları karşılaştırmak için laminar ve zamana bağlı Hesaplamalı Akışkanlar Dinamiği (HAD) analizleri gerçekleştirilmiştir.

Anahtar Kelimeler: Girdap Parçacık Yöntemi, Parçacık Gücü Değişimi, Küt Firar Kenarlı Kanat Kesitleri

To my family

ACKNOWLEDGEMENTS

First and foremost, I would like to express my sincere gratitude to my supervisor Assoc. Prof. Dr. Oğuz Uzol for his guidance, encouragements and advices.

I would like to thank all my thesis committee members; Prof. Dr. İsmail Hakkı Tuncer, Assoc. Prof. Dr. Dilek Funda Kurtuluş, Assoc. Prof. Dr. Sinan Eyi and Assoc. Prof. Dr. Özgür Kurç.

I would like to thank Ethem Hakan Orhan for his understanding and tolerance.

I am deeply thankful to Halil Kaya for his supports, encouragements and motivation throughout the study.

I would like to thank my friends for their encouragement, moral support, and suggestions. Many thanks to Şeyma Ceyhan, Eda Doğan, İmren Uyar, Emre Yılmaz and Ezgi Anık for their friendship, patience and motivation throughout my undergraduate and graduate studies.

I would like to express my endless gratitude to my family; my mother Ümran Haser and my father Memiş Haser. I wish to offer my deepest thanks to my cousin Merve Öyken who was always beside me to motivate me during the happy and tough moments of my life.

This study was supported by TUBITAK-BIDEB National Scholarship Program for MSc Students.

TABLE OF CONTENTS

LIST OF TABLES

LIST OF FIGURES

FIGURES

LIST OF SYMBOLS

c	Chord length
C_L	Lift coefficient
C_D	Drag coefficient
f	Vortex shedding frequency
h	Grid size
K	Cauchy velocity kernel
L	Characteristic length
N	Number of particles
u	Velocity
p	Pressure
PSE	Particle Strength Exchange
RW	Random Walk
RVM	Random Vortex Method
Re	Reynolds number
rms	Root mean square
St	Strouhal number
t	Time
T	Non-dimensional time
VPM	Vortex Particle Method
V	Velocity
x, y	Components of cartesian coordinates
ρ	Density
ε	Core radius
γ	Surface vorticity
ν	Kinematic Viscosity
υ	Particle volume

ω	Vorticity
Γ	Vorticity strength
ψ	Stream function
$\mathcal{G}$	Gaussian kernel

CHAPTER 1

INTRODUCTION

As power demand increases, the sizes of the wind turbines are expected to be increased. Figure 1.1 shows the relation between wind turbine size and power produced from a wind turbine. Increasing blade size raises structural concerns like increased gravitational and aerodynamic loading and economic concerns like cost of materials corresponding rise in blade size and weight. Increasing the thickness of the airfoil helps to reduce these concerns. The thicker airfoils reduce the specific weight as a function of rotor diameter and also improve structural efficiency [2]. Unfortunately, increasing the thickness of airfoils has disadvantages as well. Due to surface contamination, the boundary layer laminar to turbulent transition can occur very near to the leading edge. In order to remove the sensitivity to premature transition the airfoils can be equipped with a blunt trailing edge [3]. Airfoil with blunt trailing edge, which is also called flatback airfoil, introduces unique vortex shedding behavior due to the blunt trailing edge which acts similar to a bluff body [4]. An example for flatback airfoils is given in Figure 1. 2.

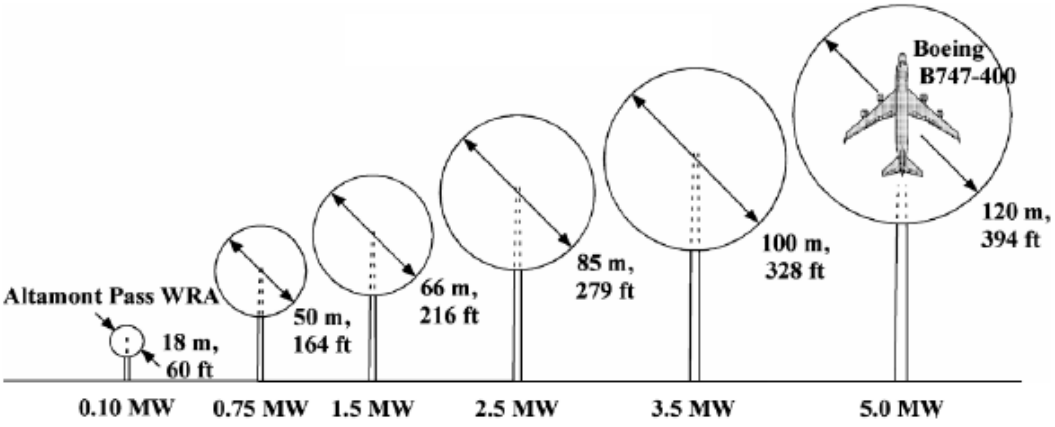

Figure 1. 1 HAWT Size and Power Trends [2]

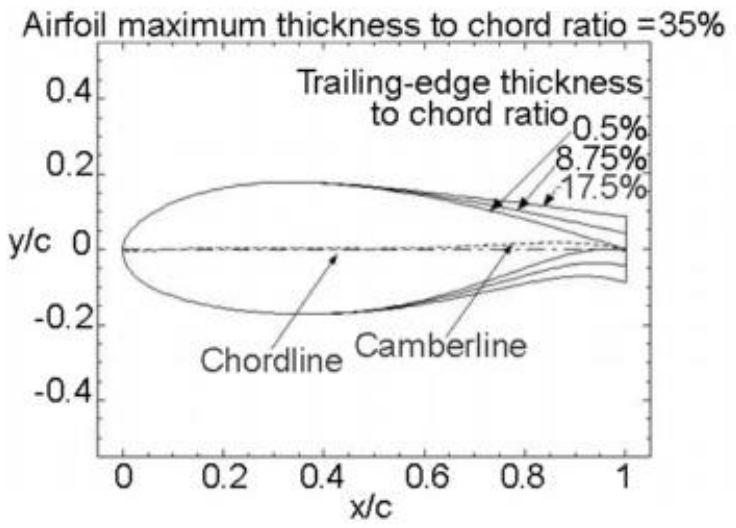

Figure 1. 2 Flatback Airfoils [5]

Bluff body areodynamics is quite different than lifting body aerodynamics. At surfaces with high curvature an adverse pressure gradient will add to the retarding action of the skin friction, which may cause the flow to be interrupted entirely and reverse in a region adjacent to the surface. This results in a region of backward flow and a detached boundary layer beyond it. At sufficiently high Reynolds numbers the

circulation region due to the separation becomes unstable. Moreover, the von Karman vortex street, which is an oscillating wake comprising large-scale eddies, forms downstream of the body. Because of the regularity of the eddy formation, the vortex shedding occurs at a dominant frequency f. This dominant frequency depends on the geometry and Reynolds number.

In bluff body aerodynamics, the interest in vortex methods boost notably. Vortex methods are based on Lagrangian numerical scheme and provide direct numerical simulation of unsteady, incompressible and viscous flows. Vortex methods for the simulation of incompressible flows have three fundamental properties [6]. First, the Navier-Stokes equations are formulated with regard to vorticity, so that the spatial discretization is achieved by using the vorticity field instead of the velocity field. In addition, the pressure drops out of the governing equation, and thus pressure term is solved only when and where force calculations are desired. Second, taking advantage of Helmholtz' theorems, in vortex methods, vortex particles are computational elements and convected with the local fluid velocity. Third, velocity field is obtained from velocity field by means of Biot-Savart law in vorticity kinematics, which allows completely describing the flow field by following vorticity elements. Another advantage of vortex methods is that different from the grid methods, no computational elements are devoted to the irrotational part of the flow. Moreover, boundary condition at the infinity is ensured automatically. Vortex methods can be faster than the Eulerian finite difference schemes by up to an order of magnitude, even when the volume is completely filled with vorticity [7].

1.1. Literature Survey

1.1.1. Vortex Methods

Vortex methods depend on a discrete Lagrangian representation of the vorticity field to satisfy the Kelvin & Helmholtz theorems approximately. The dynamics of vorticity for inviscid flows are governed by Kelvin & Helmholtz theorems [8]. Historically, simulations with vortex methods began at 1930s, with Rosenhead's calculations of Kelvin-Helmholtz instabilities [9]. The modern developments of vortex methods were started in the 1970s by Chorin [10], Leonard [11], Sarpkaya [12] and Rehbach [13]. During the early 1980s vortex methods focused on mathematical aspects like the convergence properties. In later years, researchers have concentrated on involvement of viscous effects accurately, the boundary conditions treatment at solid surfaces, and the reduction of the computational costs.

1.1.1.1. Diffusion Methods

In vortex methods, modeling diffusion is very critical issue since it includes viscous effects. There are three common diffusion methods used in vortex particle methods which are Random Walk Method, Core Spreading Model and Particle Strength Exchange Method.

The Random Walk Method (RWM) was introduced by Chorin [10] to study slightly viscous flows. The RWM simulates vorticity diffusion by pertubing the motion of vortex particles by using a Wiener process. The implementation of this method in flows with solid boundaries is easy. Leonard [11] references a study which shows that in order to model viscous diffusion accurately, the RWM requires a large number of particles compared to the Reynolds number. The problem about RWM is its low-order non-uniform convergence due to its stochastic character. This method also has statistical noise.

The Core Expansion Method was first proposed by Leonard [11]. It is a deterministic scheme which accounts for diffusion by allowing each discrete vortex core to grow at

a rate proportional to the kinematic viscosity. This formulation has simple implementation and grid-free in nature. Its convergence is better than the RWM and its scheme does not necessarily rely on the fractional step method. The inconsistency of the core spreading method is related to the treatment of the particles as solid bodies. With the core spreading method the diffusion of vorticity is approximated accurately, but the vorticity is advected with an average velocity and not with the actual local velocity. The vorticity is incorrectly convected even in the limit of infinitely many particles [6].

The Particle Strength Exchange (PSE) method is based on the general particle methods proposed by Degond and Mas-Gallic [14]. The basis of the algorithm is that the Laplacian can be replaced by an integral operator. The principal features of the PSE method are [6],

i. It is based on the exchange of circulation among particles to approximate diffusion;
ii. It involves approximating the Laplacian at a particle's location based on nearby particles,
iii. It is formulated grid-free but requires frequent remeshing of the particle field onto a well-ordered field.

PSE has been successfully used for a number of high-resolution studies. Pepin simulated flow past an impulsively started cylinder by using PSE method [8]. Koumoutsakos used PSE method to simulate the inviscid evolution of an elliptical vortex in an unbounded fluid and unsteady separated flows around circular cylinders [15]. Ploumhans and Winkelmans used PSE method to simulate flow around a square and a capsule at angle of attack. In addition, they simulated 3D flow around a sphere by using vortex method based on PSE [16], [17]. Yang analyzed flow past bridge deck sections by means of vortex method with PSE diffusion algorithm [18].

1.1.1.2. Boundary Conditions

There are two commonly used methods for the treatment of viscous boundaries in a vortex method. The first one is defining vorticity sheets at the boundary and diffusing their vorticity to free elements. The second one is defining vorticity sheets at the boundary and shedding their created vorticity on to the free elements.

Chorin [10] introduces a method for creating vorticity at boundaries and shedding this vorticity into the flow. The model of vorticity shedding away from a wall was also studied. In this method, number of particles is increasing at each time step.

Alternatively, a viscous boundary will create vorticity at its surface and release it into the flow. Methods must be created to allow the creation of vorticity of proper strength and position at each time step. The implementation of this method is studied by Koumoutsakos [15]. In this method, number of particles is kept constant.

1.1.1.3. Hybrid Methods

In hybrid schemes, Lagrangian vortex methods and Eulerian schemes rnay be combined in the same part of the domain, in which each method is used in order to discretize different parts of the governing equations.

Particle methods are grid-free methods, so that these methods are more preferable than mesh based methods for flows past complex and deforming boundaries. However the adaptivity of the Lagrangian particle methods can include errors. In order to provide consistent, efficient and accurate simulations, particle methods have to be combined with a grid. The grid does not detract from the adaptive character of the method. The function of the grid is restoring regularity in the particle locations via remeshing while it simultaneously enables systematic multiresolution particle simulations, allows fast velocity evaluations and facilitates Hybrid Particle-Mesh

methods capableof handling different numerical methods and different equations in various parts of the domain [19].

1.1.2. Flatback Airfoils

Flatback airfoils have been proposed to improve the aerodynamic performance of thick airfoils. In 1950s, Hoerner [20] presented wind tunnel results of symmetric Gö-490 airfoil with truncated trailing edge at Reynolds number of 500 000 and illustrated that truncating Gö-490 airfoil trailing edge, its maximum lift coefficient incereases. Several studies have been conducted to determine the aerodynamic effect of blunt trailing edges by Standish & van Dam [21]. Their studies are critical to understanding the effects of blunt trailing edges because they includes isolated comparisons and illustrates problems with the approach in previous studies. Prior work had typically relied on a truncation technique for the edge creation. With this technique, the rear section of a baseline airfoil is simply cut-off to create a blunt edge. Standish & van Dam [21] introduced a method of creating a blunt edge by symmetrically blending thickness on either side of the camber line in order to keep the maximum thickness and camber constant. Additionally, Winnemoller & van Dam [22] presented a numerical optimization scheme using zero-order (genetic) and first-order (gradient-based) methods resulting in a Pareto front of airfoils with significant trailing edge thicknesses.

Flatback airfoil can increase lift, trailing edge strength and resistance to performance degradation due to blade soiling, and decrease manufacturing costs [23]. However, all this comes at the expense of increased drag and increased noise due to flow separation at the trailing edge. The blunt trailing edge gives rise to drag coeffcients that negatively affect wind turbine performance. The blunt trailing edge of flatback airfoils can also lead to bluff body vortex shedding in the wake of the blade. This vortex shedding can cause rapid pressure changes which contribute to unsteady blade loading. Mertes [24] conducted experiments to observe vortex shedding of the wake behind a flatback airfoil under both static and dynamically pitching configurations.

In order to decrease drag and aerodynamic noise caused by flatback trailing edge, several passive control techniques are proposed. The use of a splitter plate is a popular method for drag mitigation due to its simplicity. It is essentially a thin plate attached at the center perpendicular to the blunt trailing edge. This modification forces the vortex sheet to be displaced further away from the edge allowing for increased base pressure. Metzinger states that drag reductions of at least 27% from the baseline were observed with the inclusion of a splitter plate length of 50% tariling edge thickness. Additionally, increasing splitter plate length was shown to continue to decrease the base drag [4].

1.2. Objective and scope

The objective of this thesis is to improve the vortex particle code developed by Kaya [1]. In the previous version of the code which Kaya [1] developed, random walk method is used to simulate vortex diffusion. In the content of this thesis, particle strength exchange method is implemented to model diffusion. Moreover, algorithm for releasing of vorticity generated on solid surface is changed. In this study, instead of generating vortex particle and sheeding them into the flow at each time step, vorticity is generated at the surface and released into flow without changing particle number. Finally, it is aimed to improve reliability of the vortex particle method code which is able to simulate flow field around bluff bodies and to analyze flatback airfoils with the developed code.

1.3. Thesis content

The thesis is organized as follows:

In CHAPTER 2, fundamental of vortex method are summarized. In CHAPTER 3, numerical implementation of vortex particle method is explained in detail. In CHAPTER 4, validation and applicability of vortex particle method code is shown

by solving general fluid dynamics problems like flow past a flat plate, a circular cylinder and a square cylinder. In CHAPTER 5, flow past flatback airfoils is simulated by using improved code. Comparisons of results obtained with present numerical implementation and CFD results are presented. Finally, in CHAPTER 6 the summary of the present study is given and future works are summarized.

CHAPTER 2

FUNDAMENTALS OF VORTEX PARTICLE METHOD

2.1. Governing Equations

Two-dimensional incompressible flow of a viscous fluid is governed by the Navier-Stokes equations, the conservation of momentum:

$$\frac{\partial \boldsymbol{u}}{\partial t} + \boldsymbol{u}.\nabla \boldsymbol{u} = -\frac{1}{\rho}\nabla p + \nu \nabla^2 \boldsymbol{u} \tag{2. 1}$$

where u is velocity of the flow, p is pressure of the flow, ρ is the fluid density and ν is the fluid kinematic viscosity. The conservation of mass:

$$\nabla.\boldsymbol{u} = 0 \tag{2. 2}$$

The vorticity is defined as the curl of the velocity.

$$\boldsymbol{\omega} = \nabla \times \boldsymbol{u} \tag{2. 3}$$

The vorticity – velocity formulation of incompressible Navier-Stokes equations is obtained by taking the curl of equation (2. 1).

$$\frac{\partial \boldsymbol{\omega}}{\partial t} + \boldsymbol{u}.\nabla \boldsymbol{\omega} = \nu \nabla^2 \boldsymbol{\omega} \tag{2. 4}$$

Rewriting equation (2. 4) in material derivative form, the following equation is obtained.

$$\underbrace{\frac{D\boldsymbol{\omega}}{Dt}}_{\text{I}} = \underbrace{\boldsymbol{\omega}.\nabla\boldsymbol{u}}_{\text{II}} + \underbrace{\nu\nabla^2\boldsymbol{\omega}}_{\text{III}} \tag{2. 5}$$

In equation (2. 5), I is convection term, II is stretching term and III is diffusion term. For two-dimensional flows, stretching term is zero. Then, equation (2. 5) becomes:

$$\frac{D\boldsymbol{\omega}}{Dt} = \nu\nabla^2\boldsymbol{\omega} \tag{2. 6}$$

Koumoutsakos proposed a fractional step algorithm for the solution of equation (2. 6). A time step Δt of the vortex method is divided into two substeps.

- Substep 1: Initially, the local velocity is computed and integrated. Then, strength of vortex particles is updated by applying particle strength exchange scheme. In this substep, no-slip boundary condition is not explicitly enforced.

  Algorithmically, substep 1 is summarized as:

$$\frac{d\boldsymbol{x}}{dt} = \boldsymbol{u}^n(\boldsymbol{x}^n, n\Delta\text{t}) \tag{2. 7}$$

$$\frac{\partial\boldsymbol{\omega_1}}{\partial t} = \nu\nabla^2\boldsymbol{\omega_1} \tag{2. 8}$$

- Substep 2: In previous substep, vorticity field ω_1 causes slip velocity on the surface. In this substep, the vortex sheet required to cancel slip velocity is computed. This vorticity sheet is emitted by the flow with the modification of vorticity field during time step Δt.

Substep 2 is expessed as:

$$\frac{\partial \boldsymbol{\omega_2}}{\partial t} - \nu \nabla^2 \boldsymbol{\omega_2} = 0 \tag{2. 9}$$

At the end of Substep 2, vorticity field ω_1 obtained in Substep 1 and vorticity field ω_2 obtained in Substep 2 are superimposed.

$$\omega^n = \omega_1 + \omega_2 \tag{2. 10}$$

2.2. Poisson Equation

In order to evolve the flow, the velocity field needs to be determined. Velocity field associated with the stream function is given as:

$$\boldsymbol{u} = \nabla \times \boldsymbol{\psi} \tag{2. 11}$$

Poisson equation is derived from equation (2. 11), the conservation of mass equation (2. 2) and vorticity equation (2. 3).

$$\nabla^2 \psi = -\omega \tag{2. 12}$$

A common approach to obtain velocity distribution from vorticity field is solving Poisson equations using Green's function. Solution of Poisson equation is given as equation (2. 13).

$$u = K * \omega = -\frac{1}{2\pi} \int K(x - y)\, x\, \omega dy + U_0 \tag{2. 13}$$

where $\boldsymbol{U_0}$ is the solution of the homogeneous Poisson equation and *K* is the Cauchy velocity kernel defined below**.**

$$K(x-y) = \frac{(x-y)}{|x-y|^2} \tag{2. 14}$$

Equation (2. 13) is also called Biot-Savart law.

2.3. Convection

Helmholtz' theorem states that vortex lines are advected with the local fluid velocity while a collocation of these lines conserves its circulation. Convection step of the vortex particle method includes the integration of local velocity field to update locations of the particles without changing strength of particles.

$$\frac{d\boldsymbol{x^{n+1}}}{dt} = \boldsymbol{u}^n(\boldsymbol{x}^n, n\Delta\mathrm{t}) \tag{2. 15}$$

2.4. Diffusion

In this thesis, Particle Strength Exchange (PSE) method is used to solve diffusion equation. In this method, the diffusion equation is satisfied by modifying the strength of the vortex particles. Diffusion equation is given as;

$$\frac{d\omega_p}{dt} = \nu\Delta\omega_p \tag{2. 16}$$

The main idea of PSE method is to replace the diffusion operator by an integral one. For this purpose, the kernel η which must satisfy the following moment properties is described [14].

$$\int x_i x_j \eta(x) dx = 2\delta_{ij} \qquad for\ i,j = 1,2,3 \tag{2. 17}$$

$$\int x_i^{i1} x_j^{i2} \eta(x) dx = 0\ if\ i_1 + i_2 = 1\ or\ 3 \le i_1 + i_2 \le r + 1 \tag{2. 18}$$

$$\int |x|^{r+2} |\eta(x)| dx < \infty \tag{2. 19}$$

Laplace operator Δ is approximated by integral operator Δ^{ε} which is defined as

$$\Delta^{\varepsilon} \omega = \varepsilon^{-2} (\eta_{\varepsilon} * \omega - \omega) \tag{2. 20}$$

where $\eta_{\varepsilon}(x) = \varepsilon^{-2} \eta(x/\varepsilon)$ is a regularization function.

Then, diffusion equation is replaced by the following integro-differential equation

$$\frac{\partial \omega}{\partial t} = \nu \varepsilon^{-2} \int [\omega(y) - \omega(x)] \eta_{\varepsilon}(x - y) dy \tag{2. 21}$$

When the integral operator is discretized using as quadrature points the locations of the particles, the equation below is obtained.

$$\frac{d\omega_p}{dt} = \nu \varepsilon^{-2} \sum_q \left(v_q \omega_q - v_q \omega_p \right) \eta_{\varepsilon}\left(\boldsymbol{x}_q - \boldsymbol{x}_p \right) \tag{2. 22}$$

where ε is core radius and v is volume of a particle.

2.5. Potential Flow Analysis in the Presence of a Vortex Cloud

In quasiy-steady flow the potential flow past a two dimensional body can be described by the boundary integral equation

$$-\frac{1}{2}\gamma(s_m)+\frac{1}{2\pi}\oint k(s_m,s_n)\gamma(s_n)ds_n+W_\infty.ds+\frac{1}{2\pi}\sum_{j=1}^{Z}L(m,j)\Delta\Gamma_j=0 \qquad (2.\ 23)$$

In equation (2. 23), the first term is the velocity discontinuity experienced when moving from the centre of the vorticity sheet onto body surface beneath [25]. The second term is the coupling coefficient. The third term is the component of freestream W_∞ parallel to the body surface at m. The last term represents the contribution to the Dirichlet boundary condition at the surface element m due to Z discrete vortices $\Delta\Gamma_j$ which form vortex cloud. The coupling coefficient, $K(s_m,s_n)$, can be written as;

$$K(s_m,s_n)=\frac{\Delta s_n}{2\pi}\left\{\frac{(y_m-y_n)cos\beta_m-(x_m-x_n)sin\beta_m}{(x_m-x_n)^2+(y_m-y_n)^2}\right\} \qquad (2.\ 24)$$

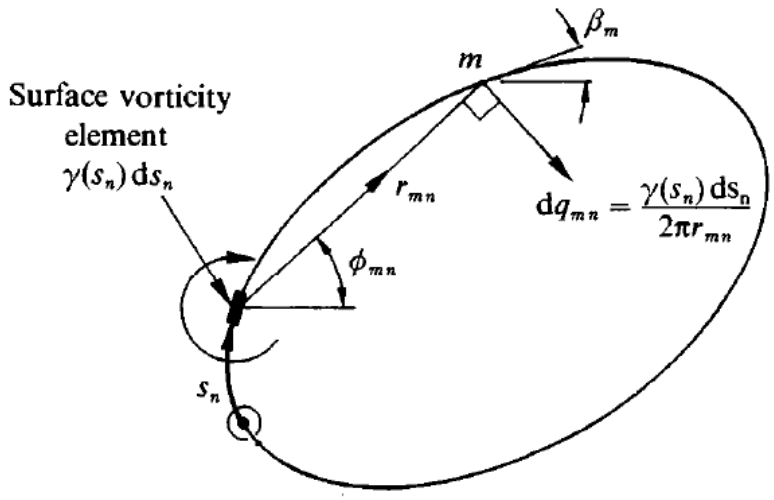

Figure 2. 1 Discrete surface vorticity model – Velocity induced by surface element s_n [25]

2.6. Surface Pressure

The determination of aerodynamic forces on solid body embedded in a fluid requires the pressure distribution on body surface. The surface pressure is obtained from vorticity flux on the surface. Conservation of momentum equation is

$$\frac{\partial \boldsymbol{u}}{\partial t} + \boldsymbol{u}.\nabla \boldsymbol{u} = -\frac{1}{\rho}\nabla p + \nu \nabla^2 \boldsymbol{u} \tag{2. 25}$$

The dot product of the momentum equation with the tangential vector of the body surface;

$$\frac{DU_s}{Dt} = -\frac{1}{\rho}\frac{\partial p}{\partial s} - \nu \frac{\partial \omega}{\partial n} \tag{2. 26}$$

where s and n denotes the tangential and normal direction of the surface panels, respectively.

Assuming that the surface velocity is constant, the equation (2. 26) reduces to;

$$\frac{1}{\rho}\frac{\partial p}{\partial s} = -\nu \frac{\partial \omega}{\partial n} \tag{2. 27}$$

where the right hand side term indicates the creation of vorticity at the surface.

$$\nu \frac{\partial \omega}{\partial n} = \frac{\partial \gamma}{\partial t} \tag{2. 28}$$

Combining equation (2. 27) and equation (2. 28) , equation (2. 29) which is an expression for pressure gradient along the solid boundary, can be obtained.

$$\frac{\partial p}{\partial s} = -\rho \frac{\partial \gamma}{\partial t} \tag{2. 29}$$

CHAPTER 3

NUMERICAL IMPLEMENTATION OF VORTEX PARTICLE METHOD

3.1. Computational Scheme

After describing fundamentals of vortex particle methods in CHAPTER 2, the computational scheme of the present code is illustrated below.

Firstly, input data which includes information about model geometry, conditions of analysis such as freestream velocity components, viscosity and time step and grid properties like grid size are loaded. At the beginning, all particles are located at grid points and their strengths are zero. Then, boundary vortices are determined by using vortex panel method and released into the flow field. Strengths of released vortex particles are distributed to vortex particles located at grid points near the boundary. After that, time step iterations start with calculation of velocity vectors of vortex particles from Biot Savart law. Then, particles are convected with these velocity vectors. Particles' locations are updated at the end of convection process. Before moving on diffusion part, strengths of particles are redistributed to gird points. During diffusion with PSE method, only strengths of particles are updated. At the end of diffusion, slip velocity is generated on the surface. Then, the boundary vortices to cancel this slip velocity are calculated and diffused into the flow. Finally, pressure distiribution and aerodynamic forces on the surface are calculated and new time step starts with calculation of vortex particles' velocity vectors.

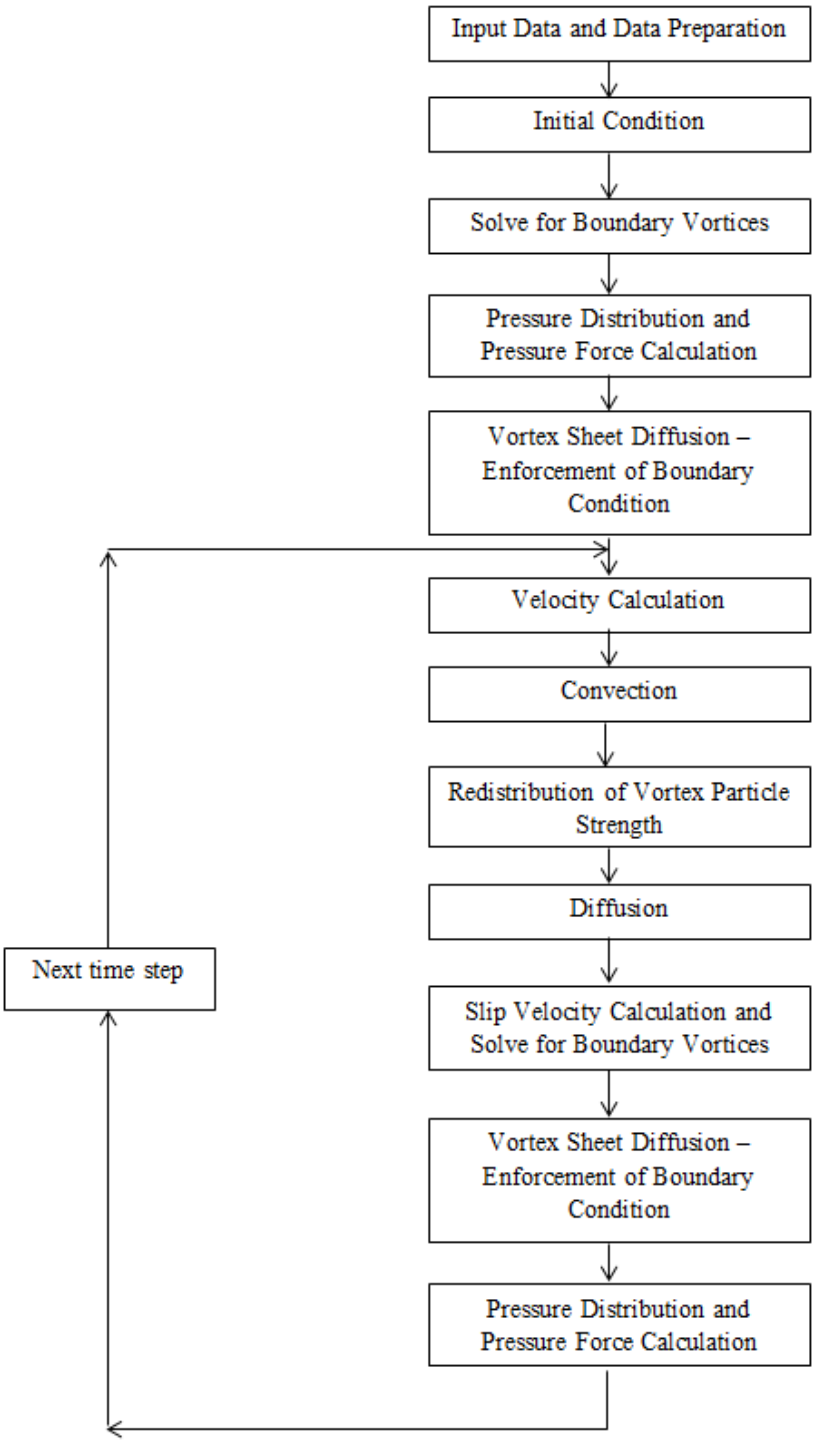

Figure 3. 1 Computational Scheme

3.2. Vortex Sheet Diffusion

Vorticities created at the wall surface is diffused into the flow by using a method proposed by Porthouse [26]. According to this method, vortex particles are released to flow field in the normal direction of wall with an offset ϵ which is a function of viscosity and time step size.

$$\epsilon = \sqrt{4\upsilon\Delta t/3} \tag{3. 1}$$

In this study, initially, vortex particles are released into the flow. Then, their vorticity values are distributed to the particles located at the nearast grid points. Distribution of particles' vorticity values is done by using Λ_1 interpolation scheme which is explained in Section 3.5.

3.3. Velocity Calculation

Using Biot-Savart law described in Section 2.2, velocity of each particle is calculated by summing up the contribution of all particles in the domain.

$$\boldsymbol{u_p} = \boldsymbol{U_0} - \frac{1}{2\pi}\sum_{i=1}^{N}\frac{\left(\boldsymbol{x_p} - \boldsymbol{x_i}\right)}{\left|\boldsymbol{x_p} - \boldsymbol{x_i}\right|^2} \times \Gamma_i \boldsymbol{k} \tag{3. 2}$$

In equation (3. 2), N is number of particles, x_p is location of particle and Γ is circulation of particle.

3.4. Convection

In this study, first order Euler scheme is used to integrate velocity field. Convection equation is given below.

$$\boldsymbol{x_i^{n+1}} = \boldsymbol{x_i^n} + \Delta t \boldsymbol{U_i}(\boldsymbol{x^n}, \Gamma^n) \tag{3. 3}$$

3.5. Redistribution of Vortex Particle Strength

In order to maintain accuracy by regulating particles and to be able to perform faster analyses a redistribution of vortex particle strength is performed. Redistribution of vortex particle strength to grids is done when one of the following cases takes place;

- Particles cease to overlap at any location of the computational domain
- Particles cluster in some region
- There are not enough to properly resolve the diffusion step

Redistribution includes interpolating vorticity field $\tilde{\boldsymbol{\omega}}$ with particles located at $\tilde{\boldsymbol{x}}$ to vorticity field $\boldsymbol{\omega}$ with particles located at $\boldsymbol{x}$. Vorticity field before redistribution ($\boldsymbol{\omega}(\boldsymbol{x})$) and after redistribution ($\tilde{\boldsymbol{\omega}}(\tilde{\boldsymbol{x}})$) should be equal.

$$\tilde{\boldsymbol{\omega}}(\tilde{\boldsymbol{x}}) \approx \boldsymbol{\omega}(\boldsymbol{x}) \tag{3. 4}$$

$$\tilde{\boldsymbol{\Gamma}}(\tilde{\boldsymbol{x}}_{\boldsymbol{i}}) \approx \sum_{\boldsymbol{j=1}}^{\boldsymbol{M}} \boldsymbol{\Gamma_j}(\boldsymbol{x_j}) \boldsymbol{\Lambda}(\tilde{\boldsymbol{x}}_{\boldsymbol{i}} - \boldsymbol{x_j}) \tag{3. 5}$$

where $\tilde{\boldsymbol{\Gamma}}$ and $\boldsymbol{\Gamma}$ denote new and old particle strengths respectively and $\boldsymbol{\Lambda}$ is interpolation kernel.

In this study, first order linear interpolation function is used for particle to mesh interpolations.

$$\boldsymbol{\Lambda_1(u)} = \begin{cases} \mathbf{1-u}, & \mathbf{0 \le u \le 1} \\ \mathbf{0}, & \boldsymbol{otherwise} \end{cases} \tag{3. 6}$$

where $u = |x|/h$. x denotes particle location and h denotes grid spacing. For two dimensional schemes, equation (3. 7) can be used.

$$\Lambda(x, y) = \Lambda(x)\Lambda(y) \tag{3. 7}$$

In this study, a rectangular grid is used. Figure 3. 2 shows Λ_1 interpolation scheme. Particles at grid points, which encircle shaded area are affected by particle to mesh interpolation.

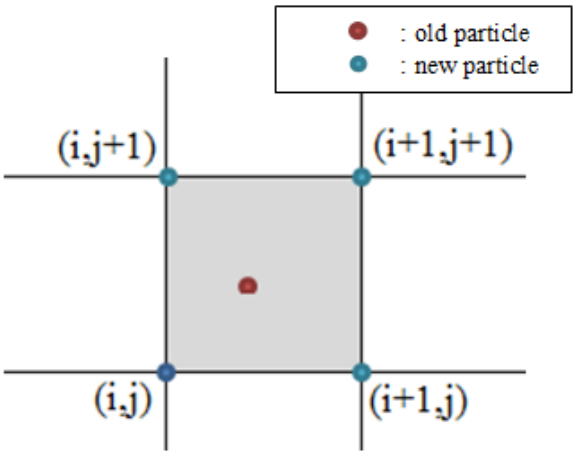

Figure 3. 2 Λ_1 scheme interpolation

3.6. Diffusion

In this thesis, diffusion of vortex particles is modelled by using Particle Strength Exchange method which is described in Section 2.4. Cottet et. al [19] state that Gaussian kernel $\mathcal{G}$ can be used in equation (2. 22) η kernel. Gaussian kernel $\mathcal{G}$ is defined as;

$$\mathcal{G}(x-y) = \frac{1}{4\pi s} e^{-(x-y)^2/4s} \tag{3. 8}$$

where $s = \nu\Delta t$.

Using Gaussian kernel and discretizing equation (2. 22) by means of explicit forward Euler scheme with a time step Δt, diffusion equation to advance from time t_n to t_{n+1} becomes;

$$\omega_p^{n+1} = \omega_p^n + \frac{1}{4\pi\varepsilon^2} \sum_q v_q \left(\omega_q - \omega_p\right) e^{-\left(x_q - x_p\right)^2/4\nu\Delta t} \tag{3. 9}$$

In diffusion subroutine, strength of particles is updated by implementing equation (3. 9).

3.7. Calculation of Boundary Vortices

After completion of convection steps in which location of particles are modified and completion of diffusion step in which strengths of particles are modified, slip velocity is generated on the solid boundary. However, for a viscous flow, normal and tangential velocity components on the solid boundary must be zero. In other words, flow must adhere to the boundary. In order to cancel slip velocity caused by particles, vorticity is generated on the solid boundary.

In this study, firstly, slip velocity on the solid boundary is calculated by using Biot-Savart law. Then, surface vorticity which ensures no-slip boundary condition is calculated by using Dirichlet type boundary condition.

Boundary vorticies at the first time step are calculated by using equation (3. 10) which is numerical form of equation (2. 23).

$$\sum_{n=1}^{M} K(s_m, s_n)\,\gamma(s_n) = -(U_\infty cos\beta_m - V_\infty sin\beta_m) - \sum_{j=1}^{Z} \Delta\Gamma_j\left(U_{mj} cos\beta_m + V_{mj} sin\beta_m\right) \quad (3.\ 10)$$

In order to calculate boundary vorticies at the next time steps, vorticity conservation equation for vortex particle models equation (3. 11) and equation (3. 10) are combined and equation (3. 12) is obtained.

$$\sum_{n=1}^{M} \gamma(s_n)\Delta s_n + \sum_{j=1}^{Z} \Delta\Gamma_j - \Gamma_{circ} = 0 \quad (3.\ 11)$$

$$\sum_{n=1}^{M} (K(s_m, s_n) + \Delta s_n)\,\gamma(s_n) = -(U_\infty cos\beta_m + V_\infty sin\beta_m) - \sum_{j=1}^{Z} \Delta\Gamma_j\left(U_{mj} cos\beta_m - V_{mj} sin\beta_m + 1\right) + \Gamma_{circ} \quad (3.\ 12)$$

The vorticies which are some distance downstream of a body are eliminated to reduce computational requirements and their effect is added to Γ_{circ} term.

3.8. Pressure Force Calculation

The expression for the pressure gradient along the solid boundary which is obtained in Section 0 can be discretized as;

$$\Delta p_i = -\rho \frac{\gamma_i \Delta s_i}{\Delta t} \tag{3. 13}$$

Moreover, the discrete pressure values at surface panels are obtained as

$$p_i = p_1 - \frac{\rho}{\Delta t} \sum_{j=1}^{i} \gamma_j \Delta s_j \tag{3. 14}$$

Using equation (3. 14), surface pressure can be calculated relative to a datum value p_1. Lewis states that pressure p_1 should be taken as zero for numerical convenience [25]. Then, the pressure at leading edge stagnation point (p_s) is searched. Then, the surface pressure values is increased by the amount of $\frac{1}{2}\rho {U_\infty}^2 - p_s$.

3.9. Parallelization

In VPM code, velocity vectors of particles are calculated by using Biot Savart law. As can be seen from equation (3. 2), velocity of one particle is affected by all of the particles in the flow field. If number of particles in the flow field is N, velocity field calculation requires work proportional to N^2. In VPM code, velocity field determination is the most time consuming part. It can be also seen from Figure 3. 3 which shows total loop time at each time step and time required for velocity calculation subroutine at each time step.

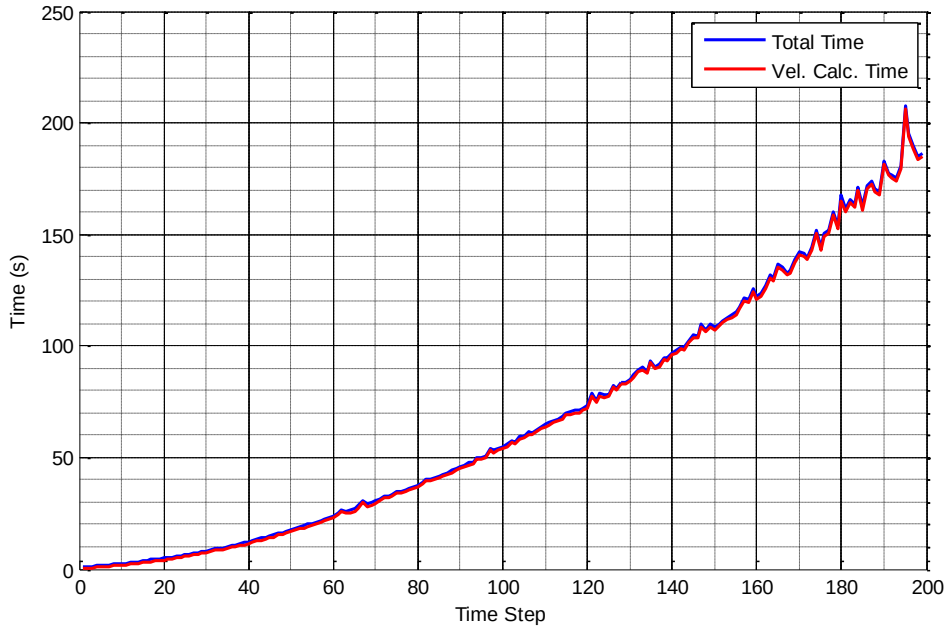

Figure 3. 3 Total loop time at each time step and time required for velocity calculation subroutine at each time step

Parallelization is only implemented to velocity calculation subroutine by using OPENMP (Open Multi-Processing) which supports multi-platform shared memory multiprocessing programming libraries.

The parallel computation of the improved method is achieved by using a shared memory system (on a workstation computer) for a test case. The computer has two Intel Xeon E5530 2.4 GHz processors. Each processor has 4 cores and 24 GB shared memory. The operating system is Microsoft Windows Vista Business. In order to test efficiency of parallelization, flow around a square cylinder with 200 panels is solved for 200 time steps by using respectively 1, 2, 4, 8 cores of the computer. Flow field of the test case includes 180 000 (300*600) grid points.

Effect of parallelization on total loop time at each time step is shown in Figure 3. 4 and the spped-up graph is given in Figure 3. 5.

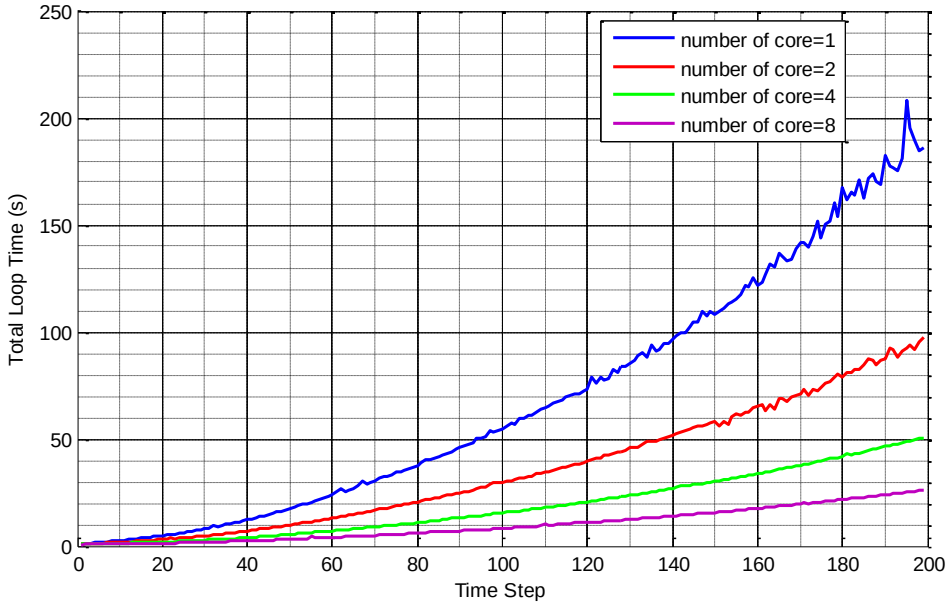

Figure 3. 4 Effect of parallelization of velocity calculation subroutine on total loop time at each time step

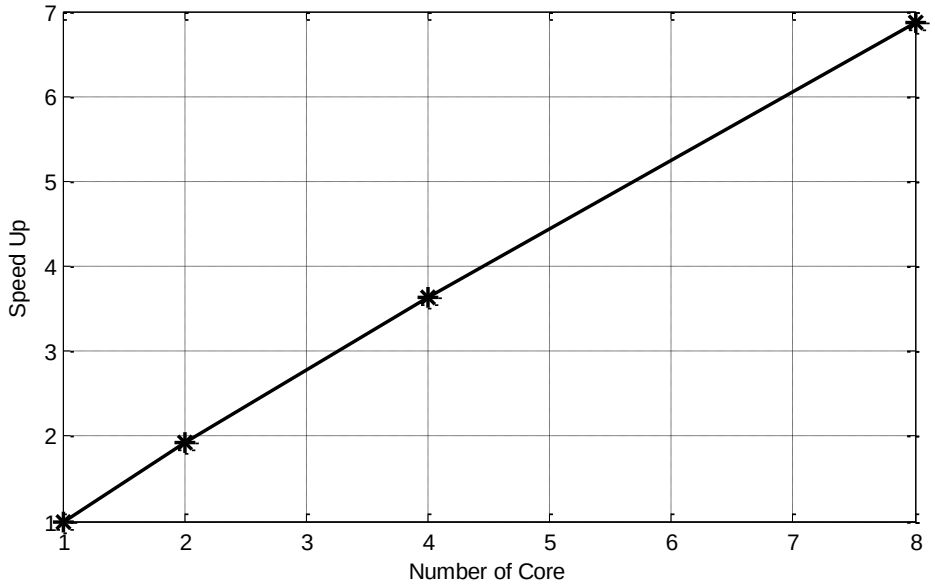

Figure 3. 5 The speed-up graph

As can be seen from Figure 3. 5, there is a linear relation between number of core and VPM code speed-up for core numbers up to 8.

CHAPTER 4

VALIDATION STUDIES

4.1. Introduction

In this chapter, the improved code is validated by solving case studies. Firstly, flow past a flat plate at Reynolds numbers of 200 and 1000 are analyzed to validate boundary layer solution of VPM code. Results are compared with Blasius boundary layer solutions. Then, flow around a circular cylinder at Reynolds number of 200 is analyzed for different panel numbers and grid sizes. VPM results which are pressure distribution, Strouhal number, lift and drag coefficients are compared with experimental and numerical results from literature. After that, flow around a square cylinder at Reynolds number of 200 is solved and results are validated with results from literature. Finally, flow around a circular cylinder at Reynolds number of 200 is analyzed by using RVM code developed by Kaya [1]. Results are compared and differences due to different diffusion methods are discussed.

4.2. Flow Past a Flat Plate

Flow past a flat plate is a fundamental test case to validate diffusion part of VPM code because boundary layer formed along an infinitely long flat plate surface is determined by viscous effects and analytical solution for this boundary layer profile is known.

4.2.1. Blasius Solution for Laminar Boundary Layer

Blasius equation for the laminar boundary layer on a flat plate is given below.

$$f.f'' + 2f''' = 0 \tag{4. 1}$$

where $f(\eta) = u(\eta)/U_\infty$ and $f' = \partial f/\partial \eta$ with η being the similarity parameter which is defined as:

$$\eta = y\sqrt{\frac{U_\infty}{\nu x}} \tag{4. 2}$$

A schematic view of flate plate with laminar boundary layer is given in Figure 4. 1.

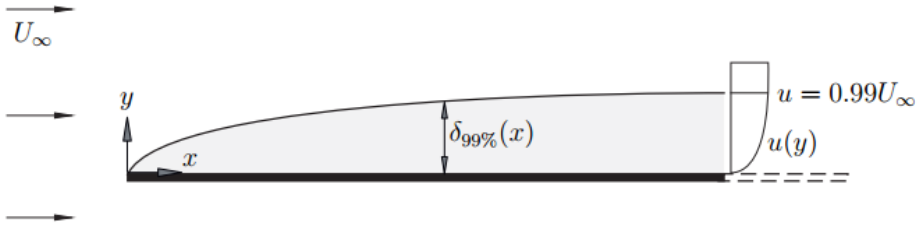

Figure 4. 1 Schematic view laminar boundary layer

4.2.2. Flat Plate at Re = 200

The flat plate having aspect ratio of 1:100 is used in simulation. Figure 4. 2 shows a snapshot of the instantaneous velocity contour plot for flow past the flat plate at Reynold number of 200. Laminar boundary layer development on the flat plate surface is observed from Figure 4. 2.

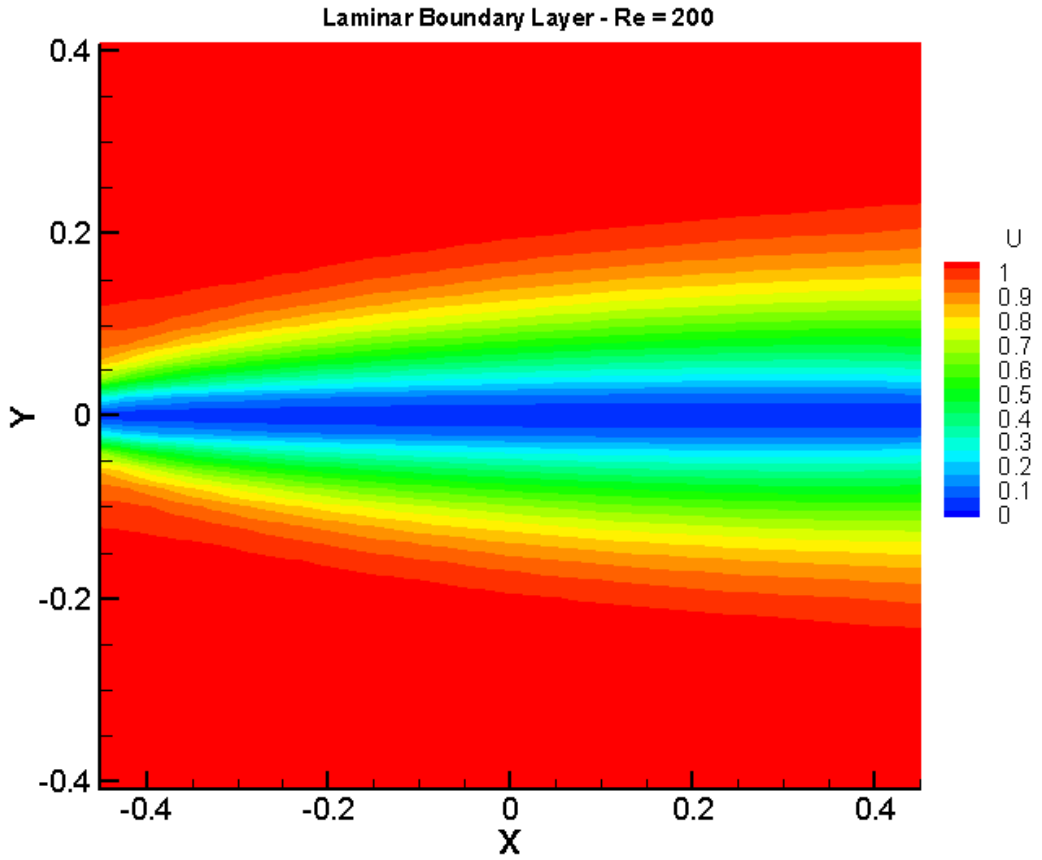

Figure 4. 2 Velocity contour of flow around flat plate at Re = 200

Figure 4. 3 shows boundary layer profiles at the 3 different locations of flat plate and comparison of results obtained from VPM code with Blasius solution. VPM results presented are time-averaged over 20 time steps. Figure 4. 3 shows that the agreement between the simulated boundary layer and the laminar Blasius solution is fairly good.

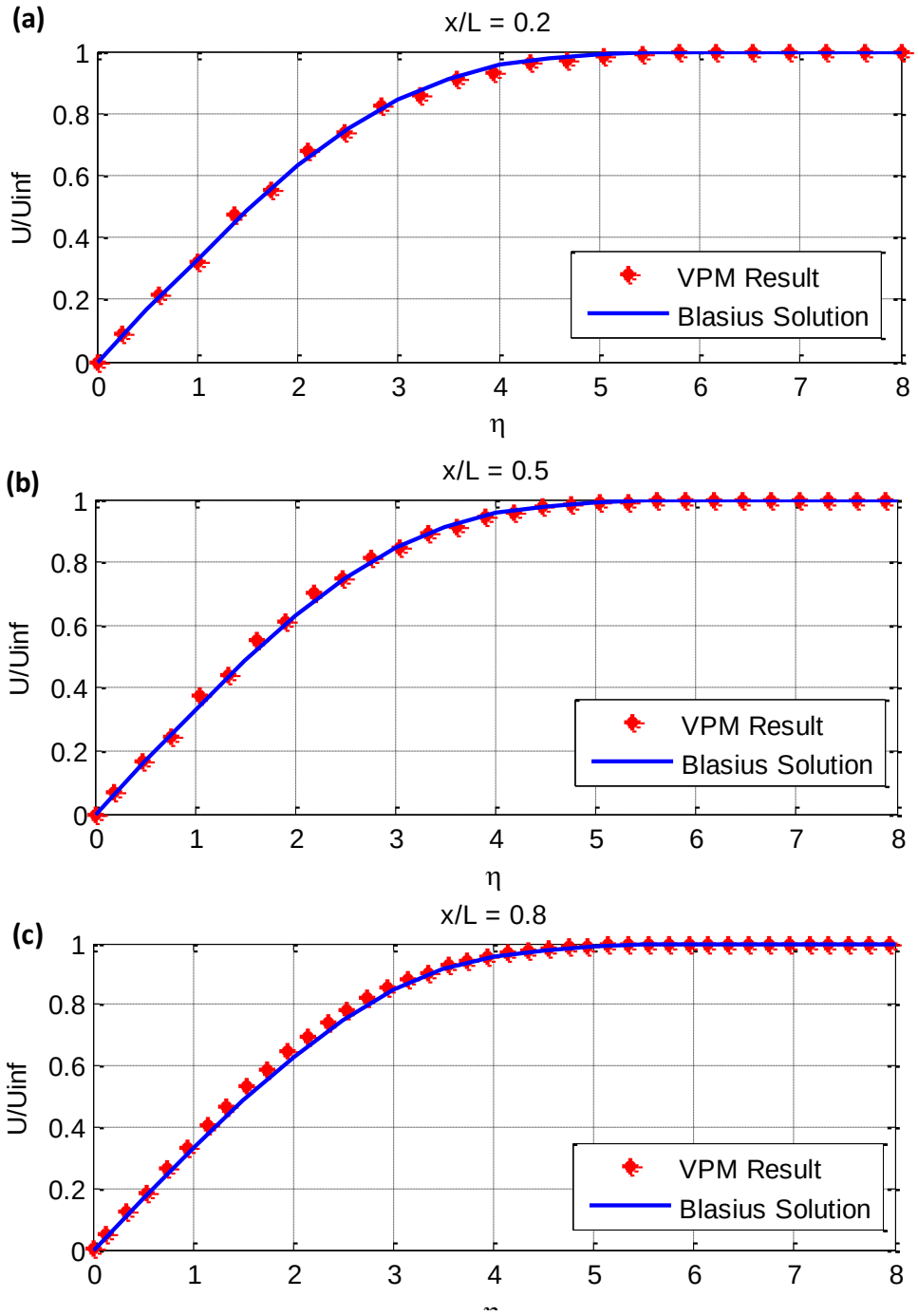

Figure 4. 3 Boundary layer profile at Re=200 – (a) x/L=0.2, (b) x/L=0.5, (c) x/L=0.8

Figure 4. 4 illustrates Blasius similarity plot for 3 different locations of flat plate and comparison of results with Blasius solution. It can be clearly seen that VPM results are well-matched with Blasius solution.

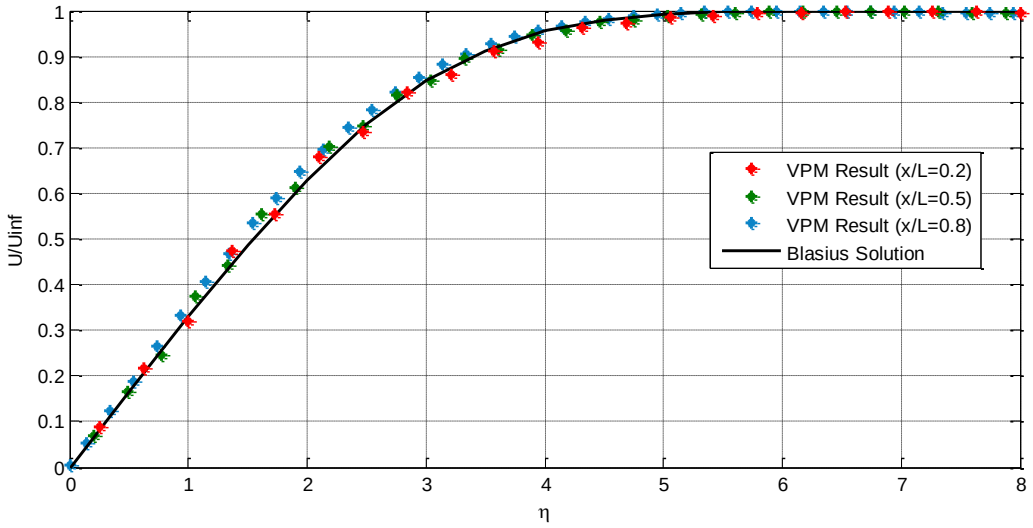

Figure 4. 4 Blasius similarity plot for 3 different locations of flat plate at Re=200

4.2.3. Flat Plate at Re = 1000

The flat plate used in this simulation has an aspect ratio of 1:100. Figure 4. 5 shows a snapshot of the instantaneous velocity contour plot for flow past the flat plate at Reynold number of 1000.

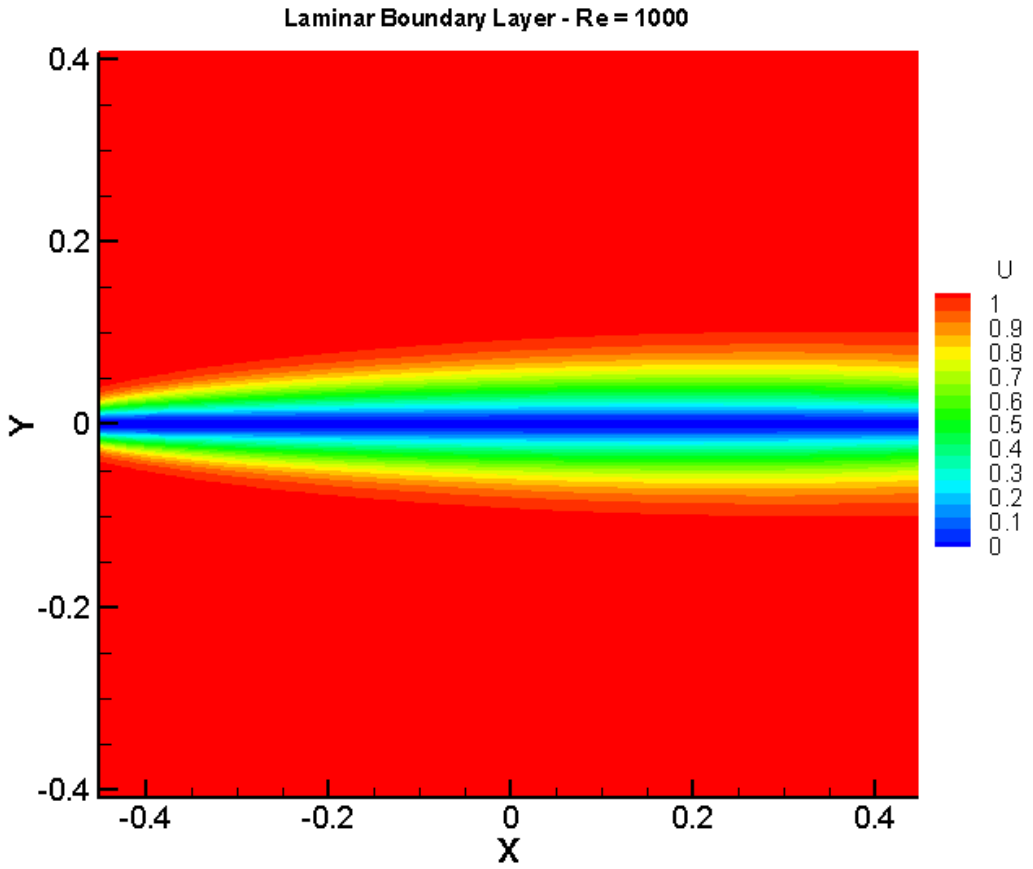

Figure 4. 5 Velocity contour of flow around flat plate at Re = 1000

Figure 4. 6 shows boundary layer profiles at the 3 different locations of flat plate which are obtained from VPM analysis and comparison of VPM results with Blasius solution. VPM results presented are time-averaged over 20 time steps. As can be seen from figure Figure 4. 6, the laminar boundary layer profile which VPM code provides is very similar to Blasius solution.

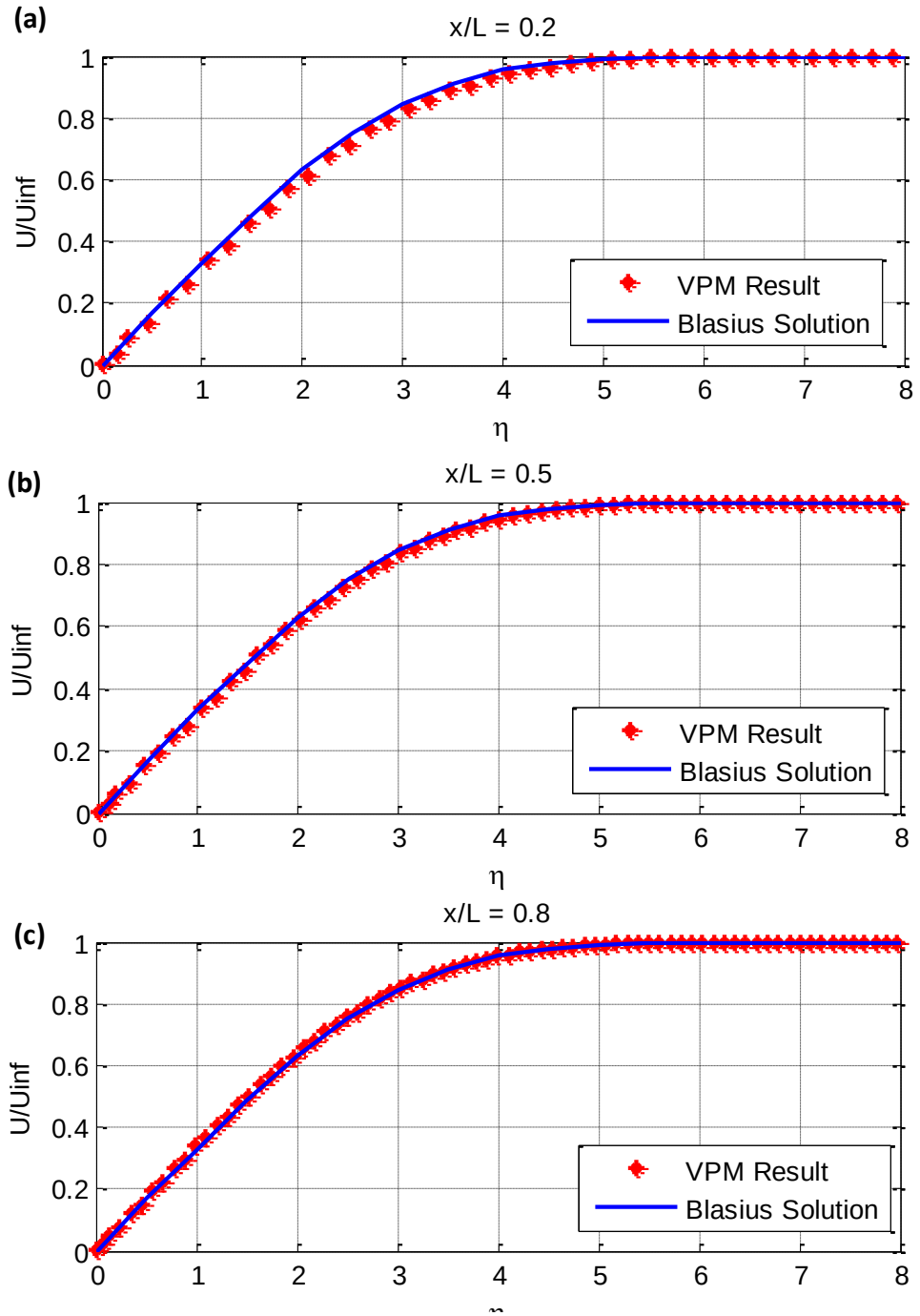

Figure 4. 6 Boundary layer profile at Re=1000 – (a) x/L=0.2, (b) x/L=0.5, (c) x/L=0.8

Figure 4. 7 illustrates Blasius similarity plot for 3 different locations of flat plate and comparison of results with Blasius solution. As can be seen, VPM results are well-matched with Blasius solution.

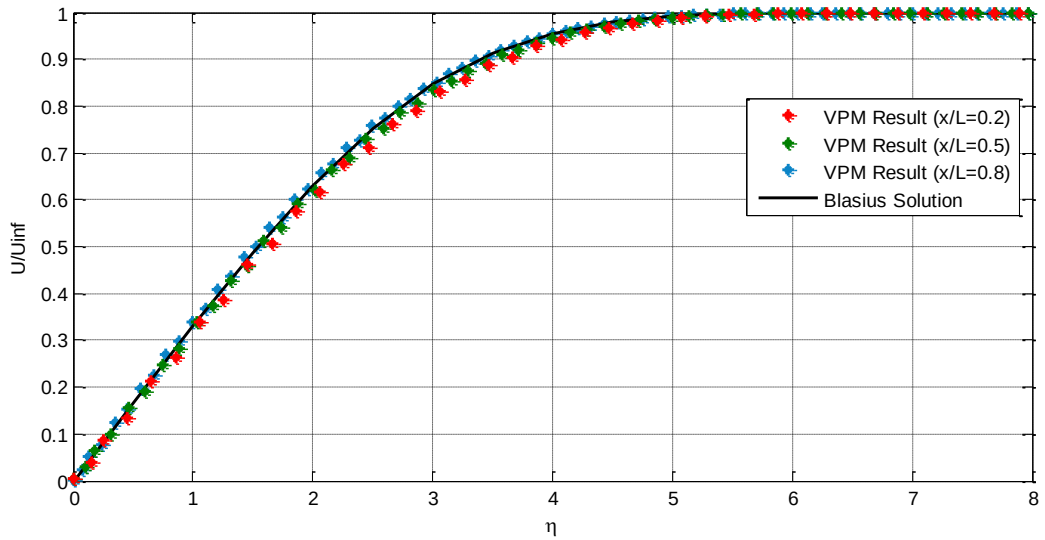

Figure 4. 7 Blasius similarity plot for 3 different locations of flat plate at Re=1000

4.3. Flow Past a Circular Cylinder

In this part of the thesis, flow past a circular cylinder is simulated by using improved VPM code. The reason for selecting this case is that there is a lot of experimental and numerical test data in literature for flow around a circular cylinder to compare VPM simulation results.

4.3.1. Convergence Study

The purpose of this study is to investigate the effect of the numerical resolution on the quality of the computed solution. The numerical experiments are conducted at Reynolds number of 200. Convergence studies are achieved for three different resolutions whih are called as coarse, medium and fine. Numerical parameters of the medium resolution case are selected such that there is a relation between grid size and time step as Koumoutsakos [15] and Pepin [8] suggested.

$$\Delta s^2 = 4\upsilon\Delta t \tag{4. 3}$$

Another consideration about selection of grid size and time step is convection. Lewis suggested that during convection, particles should go distance between half grid size an done grid size [25]. This consideration is taken into account for there resolution cases.

Numerical parameters of 3 cases are given in Table 4.1.

Table 4. 1 Numerical parameters of the convergence study

Resolution	No. of panels	Grid size	No. of grid	Time step
Coarse	100	0.08	525x350	0.08
Medium	200	0.04	1050x700	0.04
Fine	400	0.02	2100x1400	0.02

Results of lift coeficients r.m.s. values, drag coefficients and Strouhal numbers obtained with 3 different resolution cases and comparison of these results with values from literature are presented in Table 4. 2, Table 4. 3 and Table 4. 4 respectively.

Table 4. 2 Comparison of C_L r.m.s. results between VPM simulations with different resolutions and numerical values

Resolution	Present Result	2D Numerical Value [27]	Difference (%)
Coarse	0.36	0.4	10.0
Medium	0.37	0.4	7.5
Fine	0.37	0.4	7.5

Table 4. 3 Comparison of C_D results between VPM simulations with different resolutions and experimental values

Resolution	Present Result	Experimental Value [28]	Difference (%)
Coarse	1.48	1.30	13.8
Medium	1.25	1.30	3.8
Fine	1.23	1.30	5.4

Table 4. 4 Comparison of Strouhal number results between VPM simulations with different resolutions and experimental values

Resolution	Present Result	Experimental Value [29]	Difference (%)
Coarse	0.15	0.18	16.7
Medium	0.17	0.18	5.6
Fine	0.17	0.18	5.6

As can be seen from the results presented above, Strouhal number and drag coefficient cannot be predicted accurately by using coarse resolution parameters. Results obtained by using medium and fine resolutions are similar and well-matched with data from literature. When computational case is considered, fine resolution case has the highest computational cost. It can be concluded that medium resolution parameters are optimum for flow past a circular cylinder simulation at Reynolds numbers of 200.

4.3.2. Vorticity Field

Vorticity fields of flow around a circular cylinder at different non-dimensional times are given in Figure 4. 8.

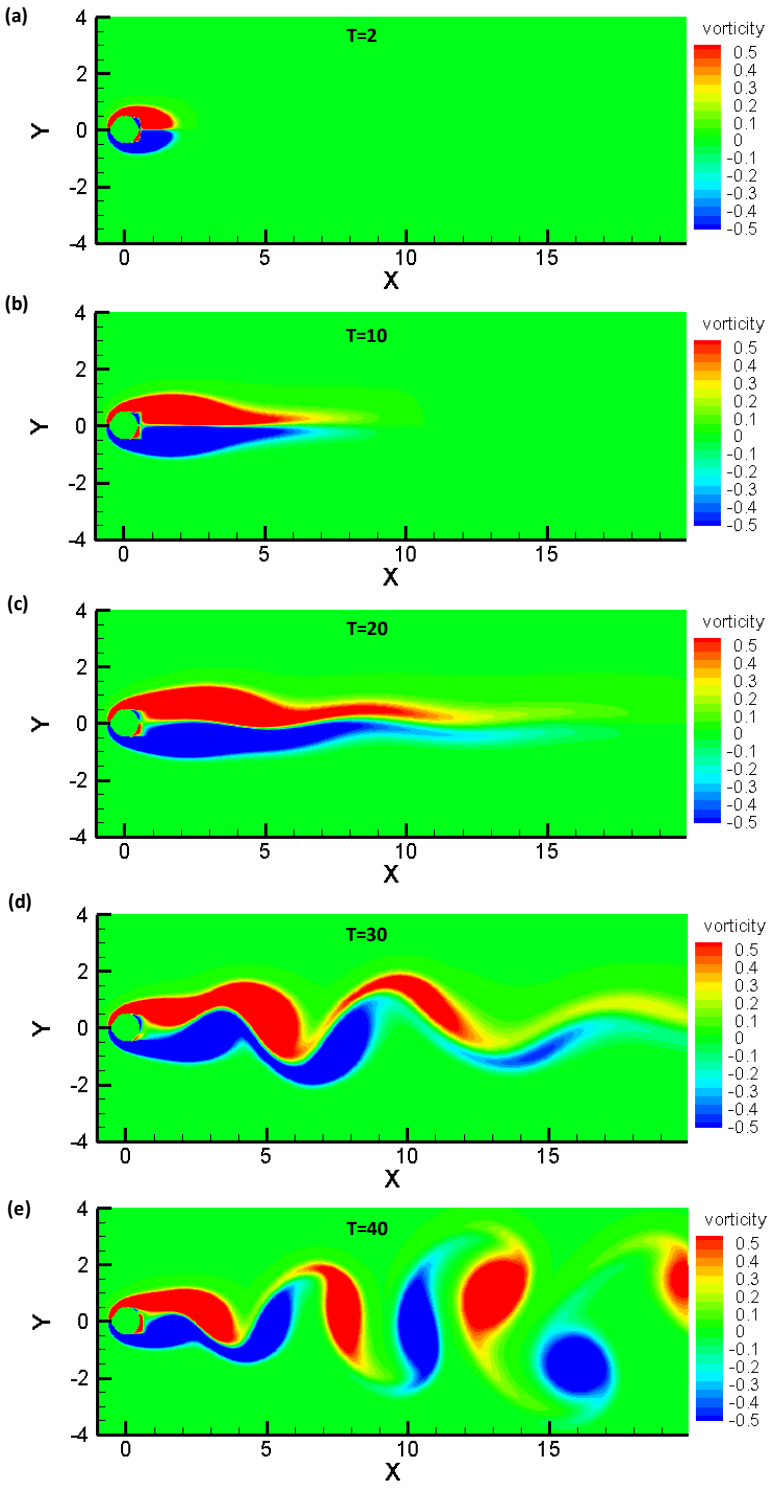

Figure 4. 8 Vorticity contours of flow past a circular cylinder at Re = 200 – (a) T = 2, (b) T = 10, (c) T = 20, (d) T = 30, (e) T = 40

4.3.3. Pressure Distribution and Force Coefficients

The comparisons for the flow around a circular cylinder case are made also with force data. It should be mentioned that, VPM calculates forces by considering only pressure forces, so viscous forces are neglected. This assumption is reasonable, because the pressure force is dominant for bluff bodies.

For flow around a circular cylinder, mean pressure coefficient distribution calculated in the medium resolution test case is given below. The comparison of pressure distribution result is made with the 2D numerical results based on finite volume method [30]. As can be seen, present pressure coefficient results and numerical values from literature are similar.

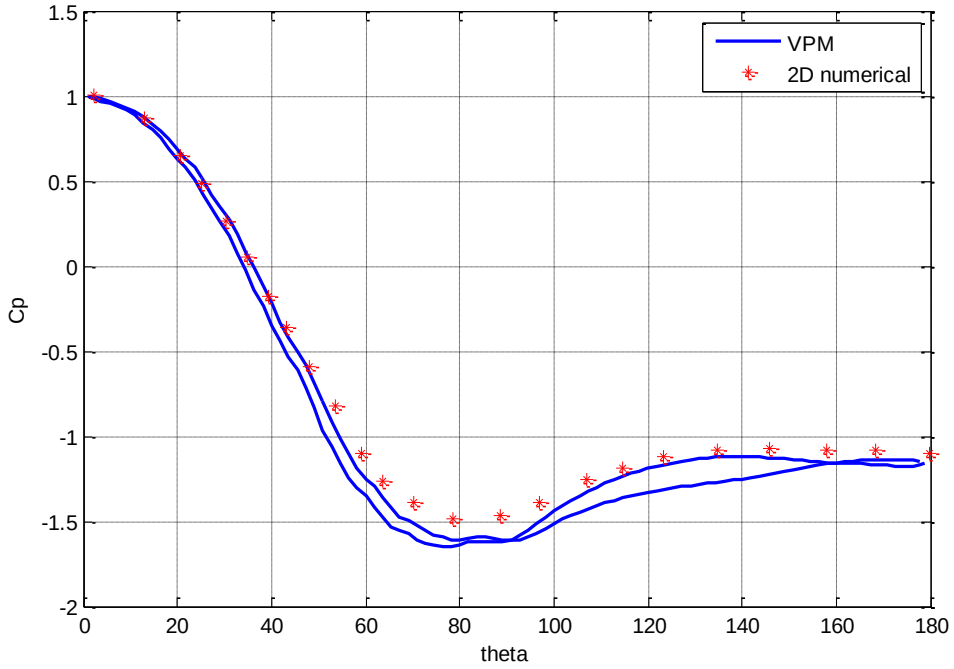

Figure 4. 9 Mean pressure coefficient distribution around a circular cylinder at Re = 200 and comparison of present results with numerical results of Rajani et. al [30]

The time history of lift and drag coefficients obtained in medium resolution case study are figured below.

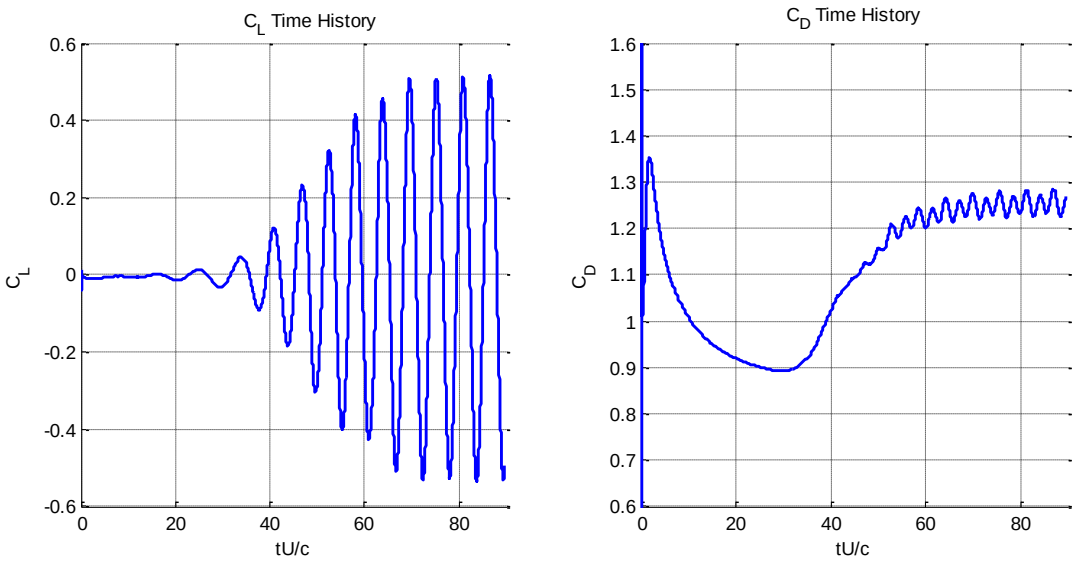

Figure 4. 10 Time histories of force coefficients for flow around a circular cylinder at Re = 200

4.3.4. Vortex Shedding Frequency

The vortex shedding frequency which are obtained with the numerical simulations, are calculated by using lift coefficient oscillations. By taking discrete Fourier transform of lift oscillations, the frequencies of vortex shedding are calculated. Then, Strouhal number is determined by averaging the dominant frequencies according to their amplitude,

$$St = \frac{fL}{V} \tag{4. 4}$$

where St is Strouhal number, f is the vortex shedding frequency and V is freestream velocity.

Single-sided amplitude spectrum of lift coefficient data of medium resolution case is given below.

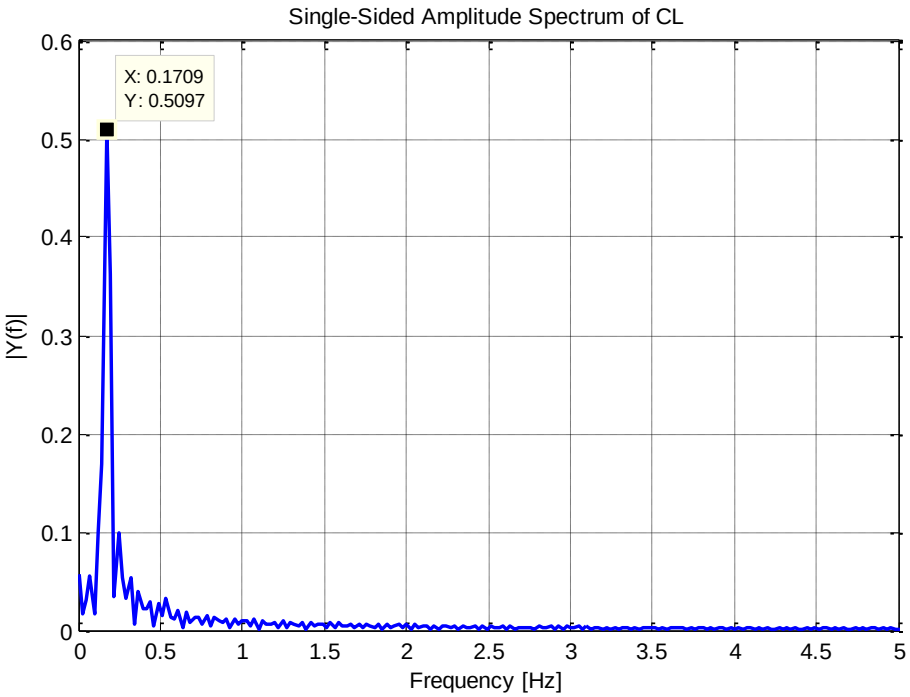

Figure 4. 11 Discrete Fourier transformation result of lift oscillation of flow around a circular cylinder at Re = 200

4.4. Flow Past a Square Cylinder

Another test case to validate VPM code is flow around a square cylinder at Reynolds number of 200. Numerical parameters of current simulation are selected same as medium resolution parameters given in Table 4. 1.

4.4.1. Vorticity Field

Vorticity fields at different non-dimensional times are given in Figure 4. 12.

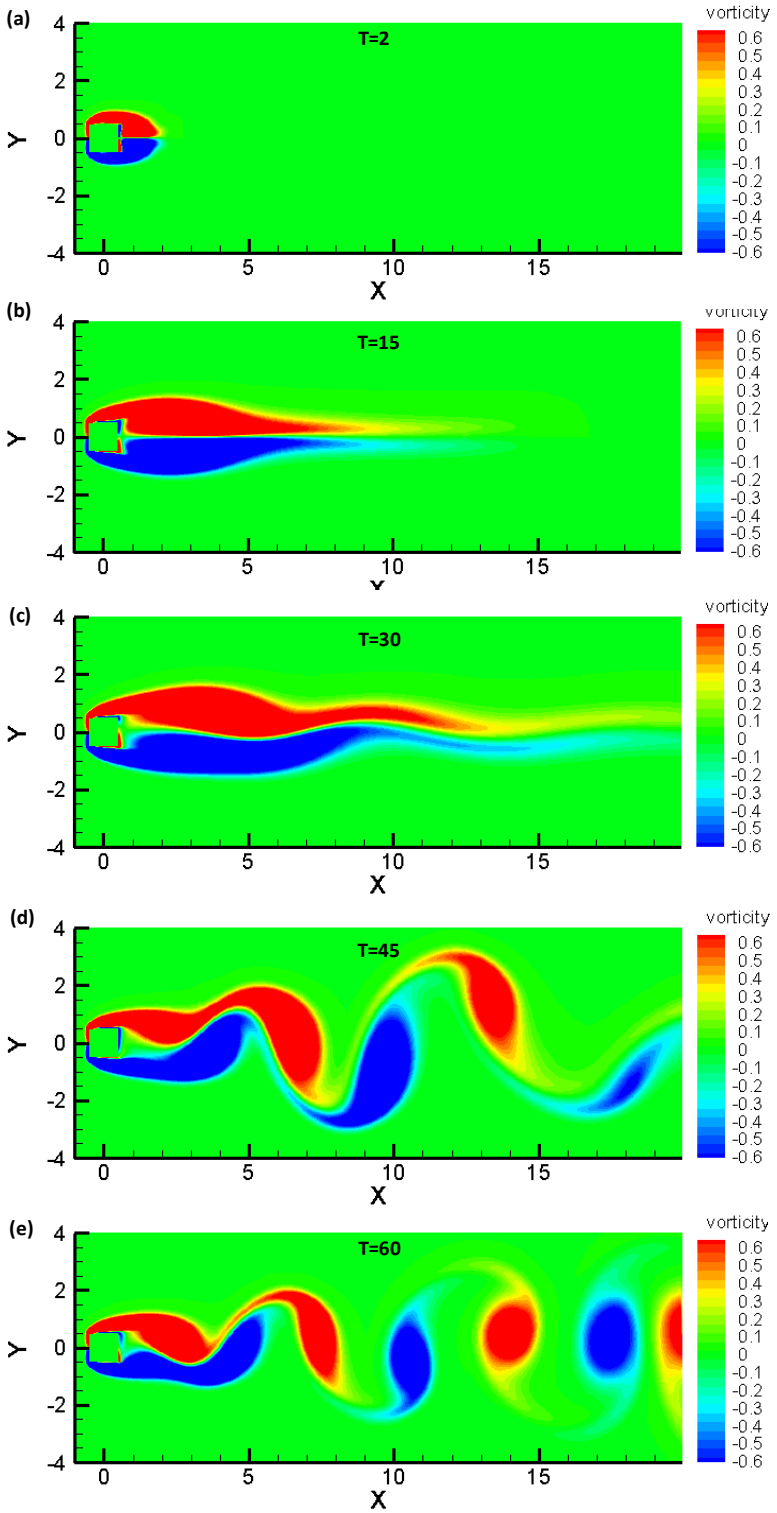

Figure 4. 12 Vorticity contours of flow past a square cylinder at Re = 200 – (a) T = 2, (b) T = 15, (c) T = 30, (d) T = 45, (e) T = 60

4.4.2. Pressure Distribution and Force Coefficients

For flow around a square cylinder case, mean pressure coefficient distribution calculated in the present study is given below. The comparison of pressure distribution result is made with the 2D numerical results [31]. It can be seen that present pressure coefficient results and numerical values from literature are matched well.

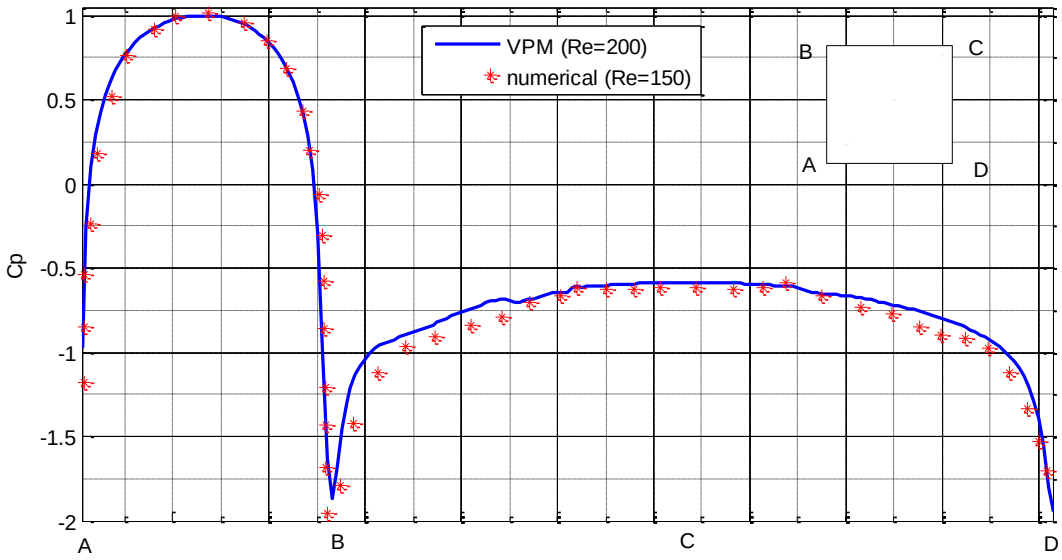

Figure 4. 13 Mean pressure coefficient distribution around a square cylinder at Re = 200 and comparison of present results with numerical results of Yoon et. al [31]

The time history of lift and drag coefficients obtained in present study are figured below.

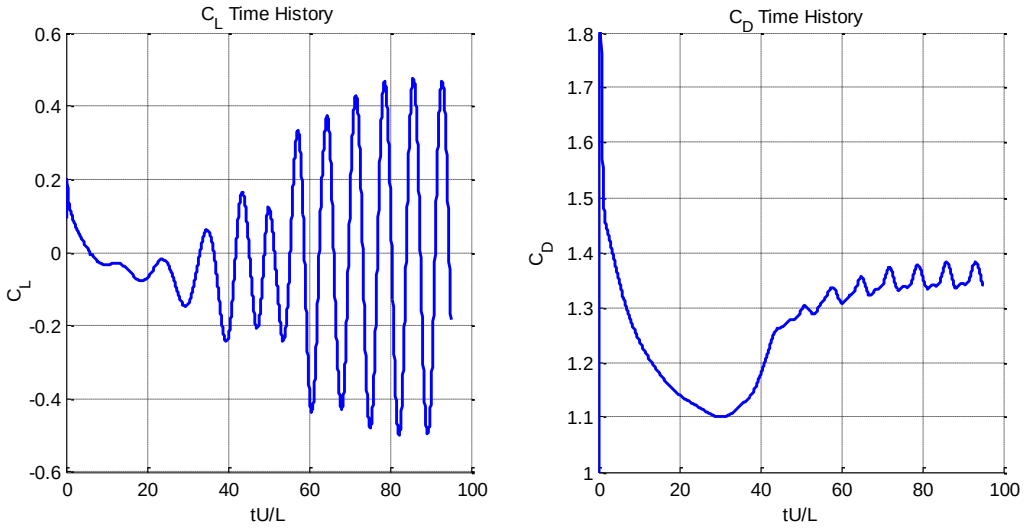

Figure 4. 14 Time histories of force coefficients for flow around a square cylinder at Re=200

Sohankar [32] compiled the drag coefficient values from different numerical and experimental studies in literature. Figure 4. 15 shows these drag coefficients at different Reynolds numbers for a square cylinder.

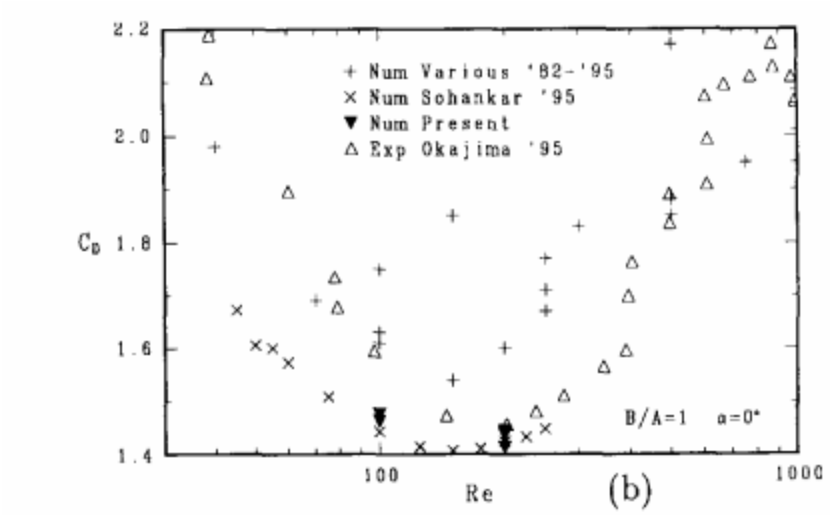

Figure 4. 15 Variation of drag coefficient with Reynolds number for a square cylinder [32]

Comparison of present drag coefficient and root mean square of lift coefficient with the values in literature are presented in Table 4. 5 and Table 4. 6, respectively. Comparisons show that present results are in good agreement with values in literature.

Table 4. 5 Comparison of the present drag coefficient result with experimental value in literature

	Present Result	**Experimental Value** [32]	**Difference (%)**
C_D	1.37	1.45	5.5

Table 4. 6 Comparison of the present lift coefficient rms result with numerical value in literature [33]

	Present Result	**Experimental Value** [33]	**Difference (%)**
C_L rms	0.365	0.377	3.2

4.4.3. Vortex Shedding Frequency

Strouhal number is determined from time history of lift coefficient. Discrete Fourier transform of lift coefficient is calculated to obtain vortex shedding frequency (Figure 4. 16).

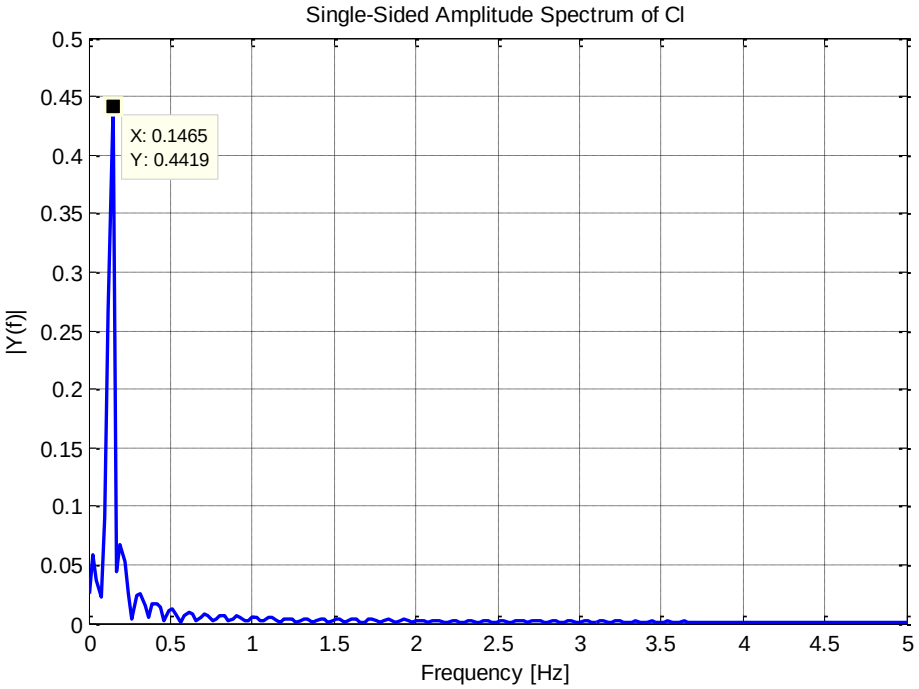

Figure 4. 16 Discrete Fourier transformation result of lift oscillation of flow around a square cylinder at Re = 200

Figure 4. 17 illustrates the experimental results about the relation between Strouhal number and Reynolds number for a square [34]. According to this figure, Strouhal number of flow past a square at Reynolds number of 200 obtained by VPM is very close to experimental value in Figure 4. 17.

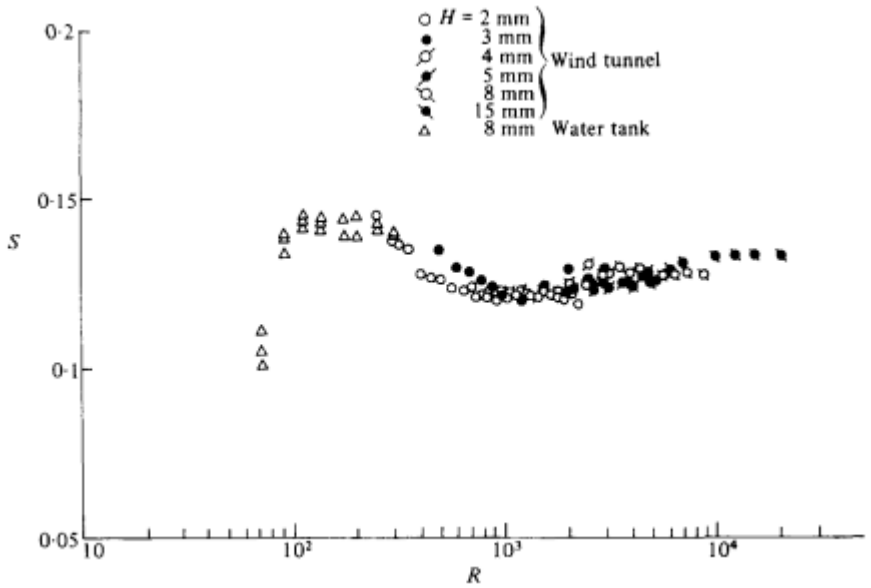

Figure 4. 17 Variation of Strouhal number with Reynolds number for a square cylinder [34]

Table 4. 7 Comparison of the present Strouhal number result with experimental value in literature [34]

	Present Result	**Experimental Value [34]**	**Difference (%)**
Strouhal number	0.147	0.145	1.4

4.5. Comparison of Random Walk Method and Particle Strength Exchange Method

As explained in Section 1.1.1, Random Walk method is a stochastic method, whereas Particle Strength Exchange method is deterministic. Random Walk method has statictical noise and low rate of convergence. Koumoutsakos solved a 1D diffusion problem, by using Random Walk (RW) and Particle Strength Exchange (PSE)

methods of diffusion and he compared results with analytical results [15]. Figure 4. 18 illustrates comparison of results.

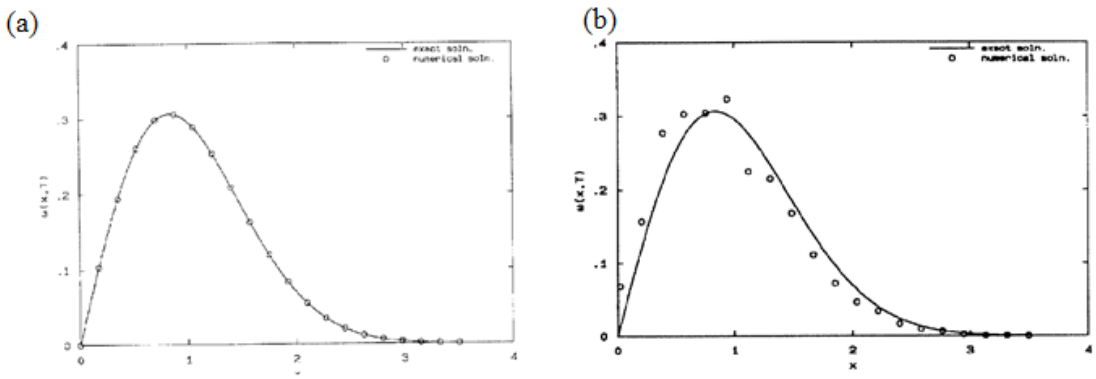

Figure 4. 18 Comparison of PSE and RW methods for a 1D diffusion problem [15] – (a) Comparison of PSE result with exact solution, (b) Comparison of RW result with exact solution

As can be seen, result obtained by using PSE algoritm and exact solution are matched well. PSE result does not have any noise, whereas RW result is noisy.

Flow around a circular cylinder at Reynolds number of 200 is simulated by using RVM algoritm developed by Kaya and includes diffusion Random Walk algorihm [1] and results are compaired with the results obtained by VPM algorithm, which includes diffusion with PSE, in Section 4.3.

Figure 4. 19 ilustrates the time history of oscillating part of lift and drag coefficients obtained by means of VPM and RVM.

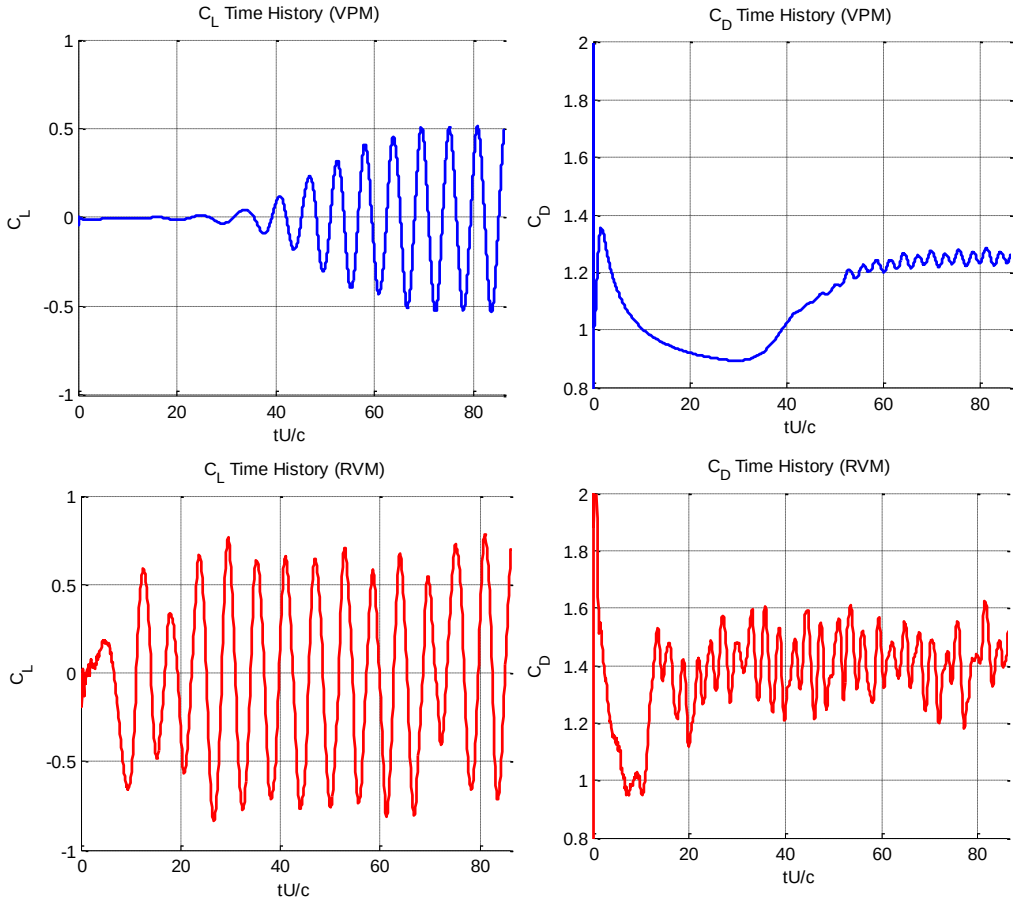

Figure 4. 19 Time histories of force coefficients for flow around a circular cylinder at Re = 200 obtained by using VPM and RVM methods

As can be seen from Figure 4. 19, RVM provides noisy results. Because of randomness of the diffusion, oscillations start much earlier in RVM simulation. Moreover, amplitudes of lift coefficient oscillations obtained by RVM have not regular behavior as VPM results have.

Results of lift coeficients r.m.s. values, drag coefficients and Strouhal numbers obtained with VPM and RVM algorithms and comparison of these results with values from literature are presented in Table 4. 8, Table 4. 9 and Table 4. 10 respectively.

Table 4. 8 Comparison of C_L r.m.s. results of VPM and RVM simulations and numerical values from literature

Method	**Present Result**	**2D Numerical Value** [27]
VPM	0.37	0.4
RVM	0.48	0.4

Table 4. 9 Comparison of C_D results of VPM and RVM simulations and experimental values from literature

Method	**Present Result**	**Experimental Value** [28]
VPM	1.25	1.30
RVM	1.40	1.30

Table 4. 10 Comparison of Strouhal number results of VPM and RVM simulations and experimental values from literature

Method	**Present Result**	**Experimental Value** [29]
VPM	0.17	0.18
RVM	0.17	0.18

Comparison of results shows that Strouhal numbers obtained by VPM and RVM are same. However, RVM overpredict drag coefficient and r.m.s. value of lift coefficient.

CHAPTER 5

AERODYNAMIC ANALYSIS OF FLATBACK AIRFOILS

5.1. Introduction

In this thesis, aerodynamic analysis of FB3500-1750 flatback airfoil, which is commonly used in wind turbine airfoil investigations, is carried out by means of Vortex Particle Method (VPM). Coordinates of FB3500-1750 airfoil are found in literature. FB3500 series flatback airfoils are obtained by adding thickness to both sides of the airfoil from maximum thicknesss location to trailing edge. In order to investigate effect of trailing edge thickness on aerodynamic parameters FB3500-2250 flatback airfoil is generated. FB3500 flatback airfoil series are given below.

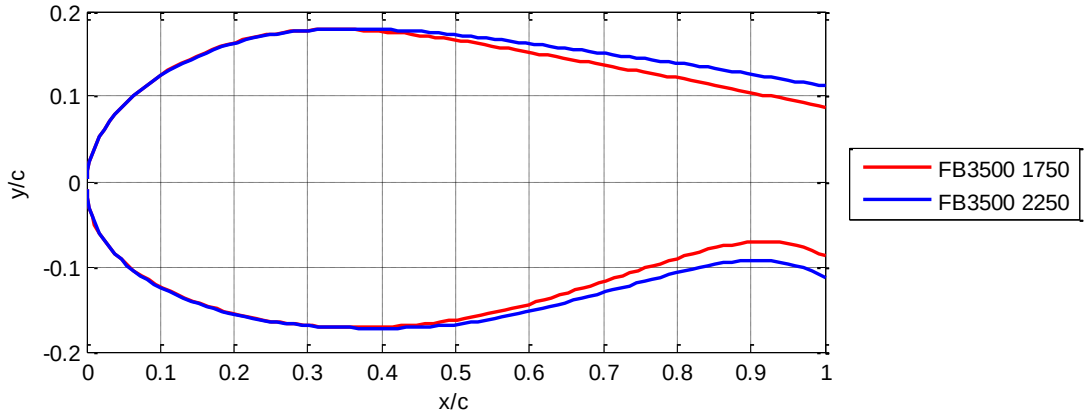

Figure 5. 1 FB3500 Flatback Airfoil Series

Literature survey about flatback airfoils shows that flow around flatback airfoils is usually investigated for Reynolds number higher than 600 000. VPM code which is

developed in the content of this thesis is a laminar solver, so that it is not able to solve turbulent flow accurately. Thus, VPM analyses are done for Reynolds number of 1000 at 0º angle of attack. In order to compare VPM results, unsteady CFD analyses are employed.

CFD analyses are performed with FLUENT software. Laminar, pressure based, implicit and node based solver is used for analyzing flow field around the flatback airfoils. The unsteady computations are carried out until a steady or a periodic behavior in aerodynamic coefficients is observed.

5.2. Computational Grids for CFD Analysis

Computational grid used in CFD analyses is illustrated in Figure 5. 2. Near the solid boundary, grids are structured. For the rest of the computational domain, unstructured grids are generated. The computational grid is refined at the airfoil wake location to prevent numerical diffusion.

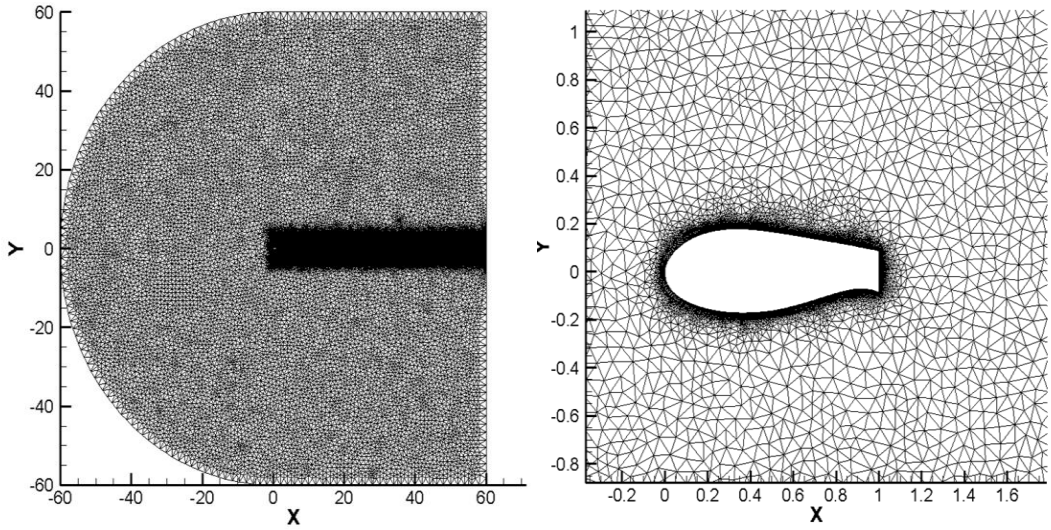

(a) (b)

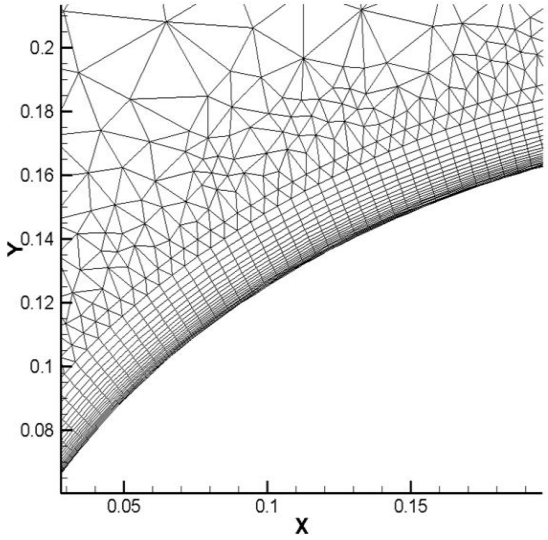

(c)

Figure 5. 2 Computational domain used in CFD analyses (a) Computational domain (b) Zoomed view of computational domain (c) Grid near the solid boundary

Cartesian grid with uniform grid size is used in VPM analyses. In Figure 5. 3, a zoomed view of computational domain used in VPM analyses is given. In VPM analysis, flow variables at grid points inside the model are set zero, so that these grid points are ignored during the calculations.

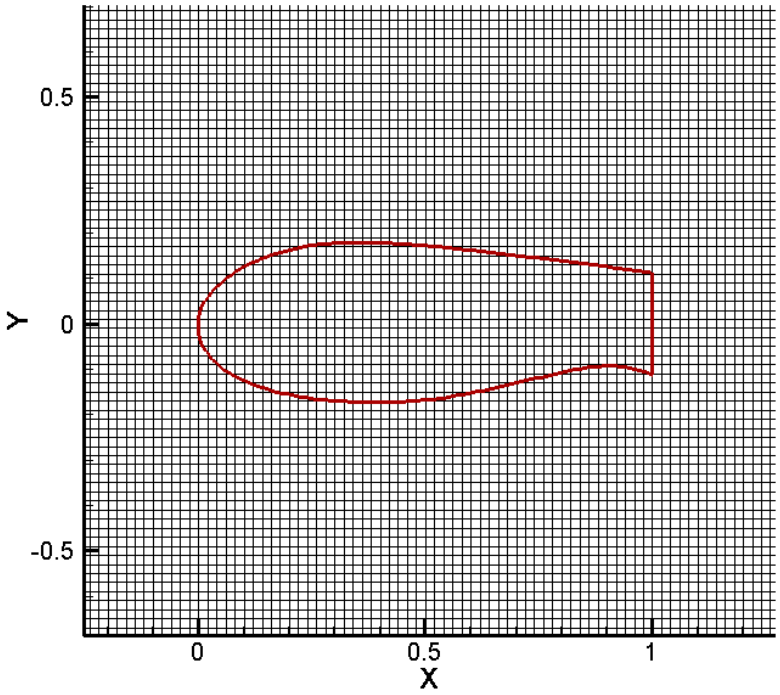

Figure 5. 3 Zoomed view of computational domain used in VPM analyses

5.3. Vorticity Field

Vorticity fields of FB3500-1750 and FB3500-2250 airfoils at different non-dimensional times are given Figure 5. 4 and Figure 5. 5 respectively.

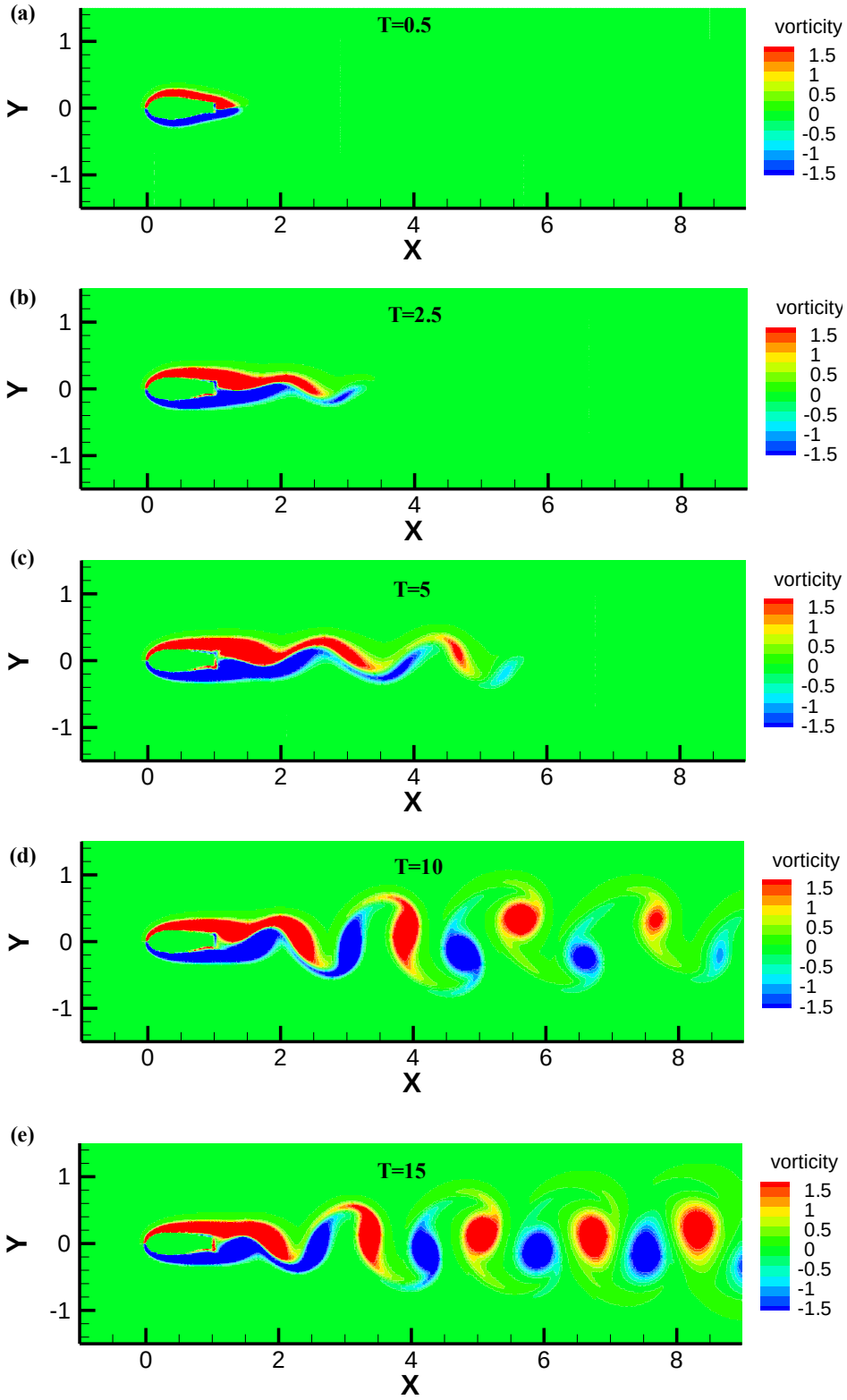

Figure 5. 4 Vorticity contours of flow past a FB3500-1750 flatback airfoil at Re = 1000 – (a) T = 0.5, (b) T = 2.5, (c) T = 5, (d) T = 10, (e) T = 15

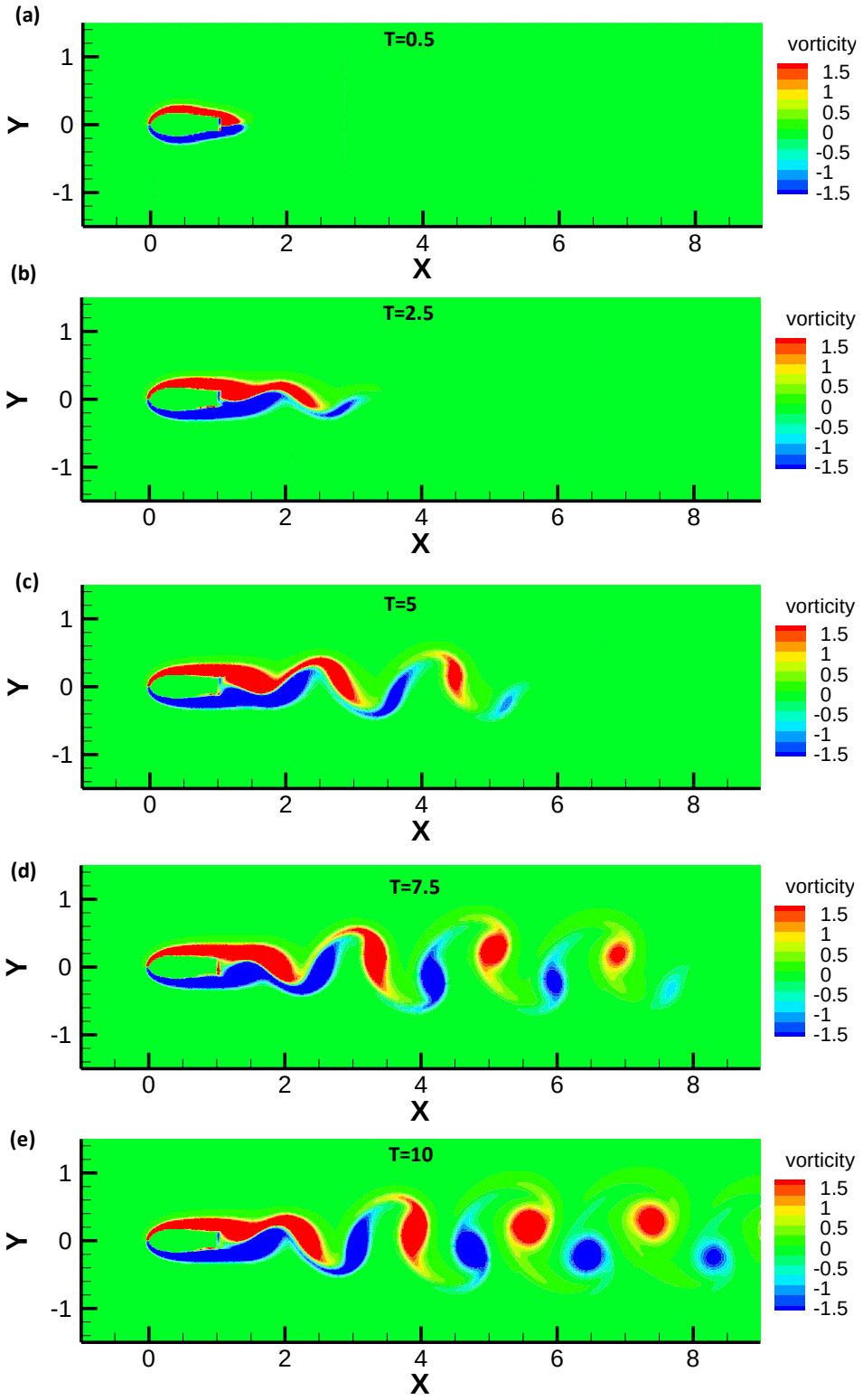

Figure 5. 5 Vorticity contours of flow past a FB3500-2250 flatback airfoil at Re = 1000 – (a) T = 0.5, (b) T = 2.5, (c) T = 5, (d) T = 7.5, (e) T = 10

5.4. Pressure Distributions

For flow around flatback airfoil cases, mean pressure coefficient distribution calculated in the present study is given below.

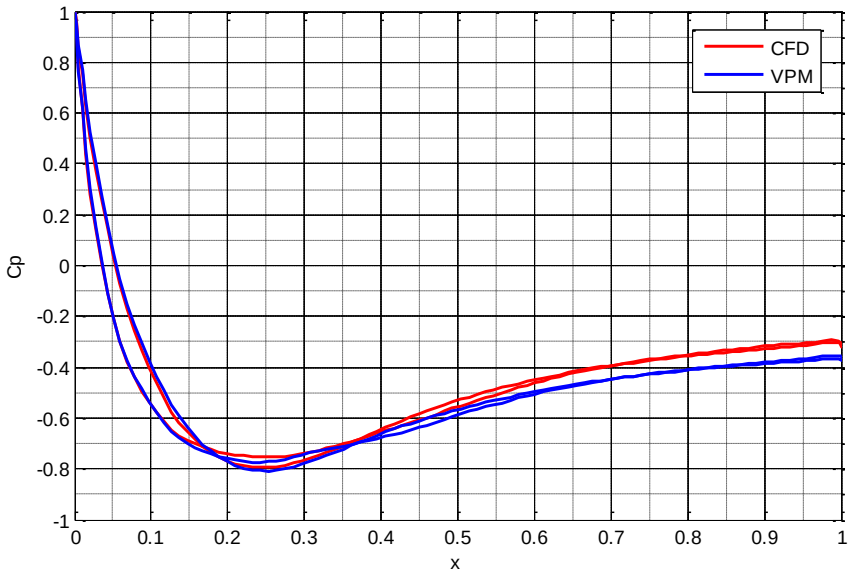

Figure 5. 6 Mean pressure coefficient distribution around FB3500-1750 flatback airfoil at Re = 1000 – VPM and CFD results

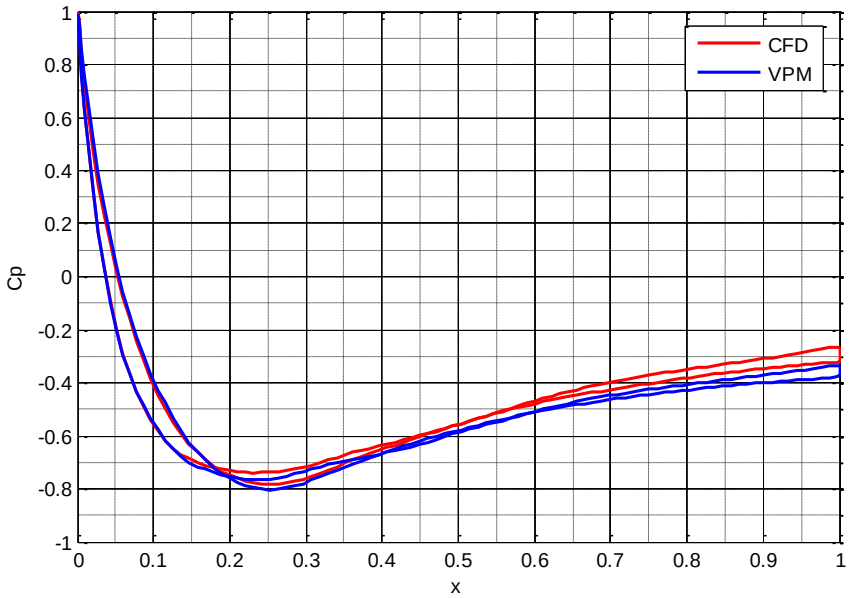

Figure 5. 7 Mean pressure coefficient distribution around FB3500-2250 flatback airfoil at Re = 1000 – VPM and CFD results

As can be seen from figures, pressure distributions obtained from CFD and VPM are in fairly good agreement. Minimum pressure coefficient values calculated by CFD and VPM are similar. There is a small difference between base pressure values which explains difference in drag coefficient values.

Pressure coefficient distributions of FB3500-1750 and FB3500-2250 airfoils at different non-dimensional times are given Figure 5. 8 and Figure 5. 9 respectively.

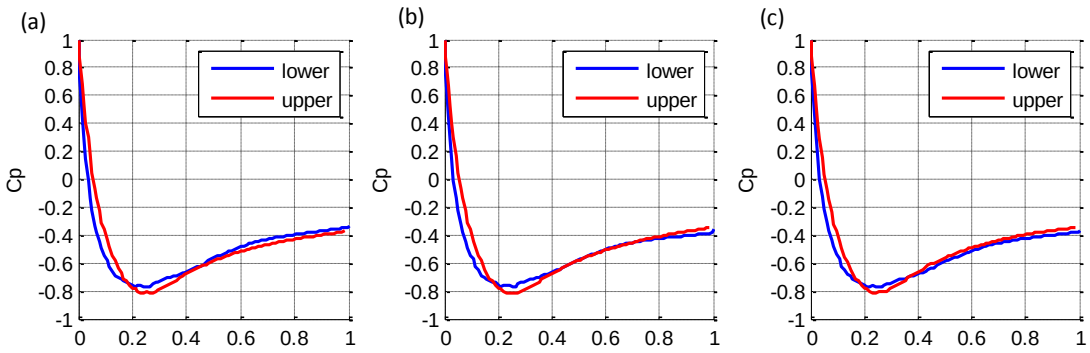

Figure 5. 8 Pressure coefficient distributions of flow past a FB3500-1750 flatback airfoil at Re = 1000 – (a) T = 18.9, (b) T = 19.5, (c) T = 20

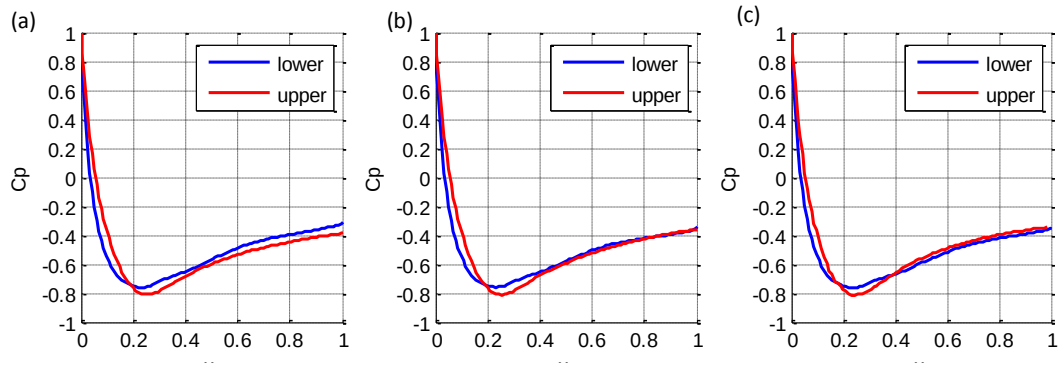

Figure 5. 9 Pressure coefficient distributions of flow past a FB3500-2250 flatback airfoil at Re = 1000 – (a) T = 27.0, (b) T = 27.2, (c) T = 27.4

5.5. Force Coefficients and Vortex Shedding Frequency

Figure 5. 10 and Figure 5. 12 show time history of lift coefficient and drag coefficient at Reynolds number of 1000 obtained from VPM analyses for FB3500-1750 and FB3500-2250 flatback airfoils respectively.

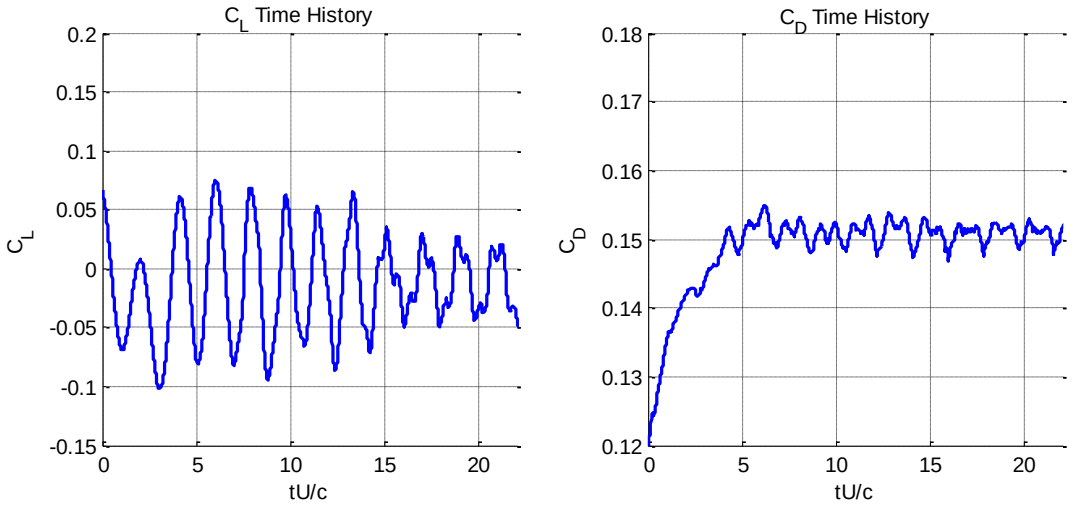

Figure 5. 10 Time histories of force coefficients for flow around FB3500-1750 flatback airfoil at Re = 1000 – VPM result

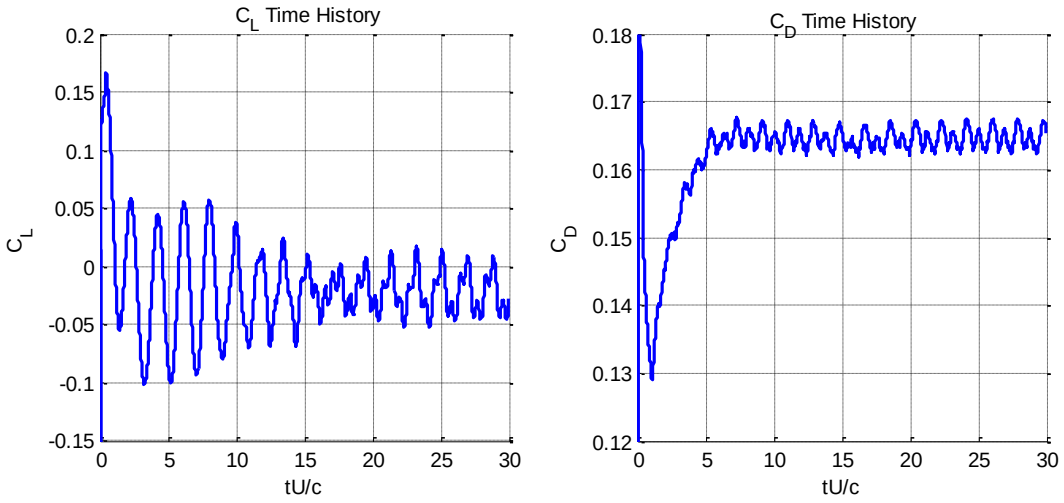

Figure 5. 11 Time histories of force coefficients for flow around FB3500-2250 flatback airfoil at Re = 1000 – VPM result

Singel-sided amplitude spectrums of lift coefficient data for FB3500-1750 and FB3500-2250 flatback airfoils are given below.

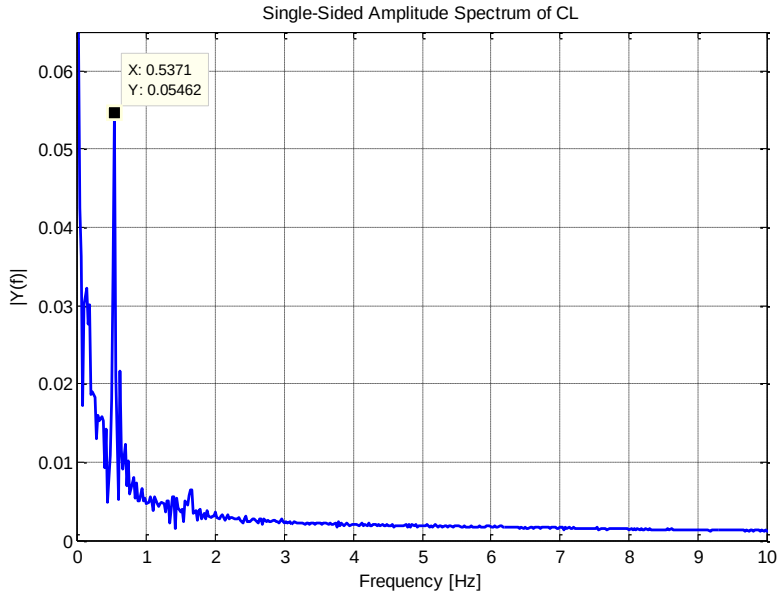

Figure 5. 12 Discrete Fourier transformation result of lift oscillation of flow around a FB3500-1750 flatback airfoil at Re = 1000 – VPM result

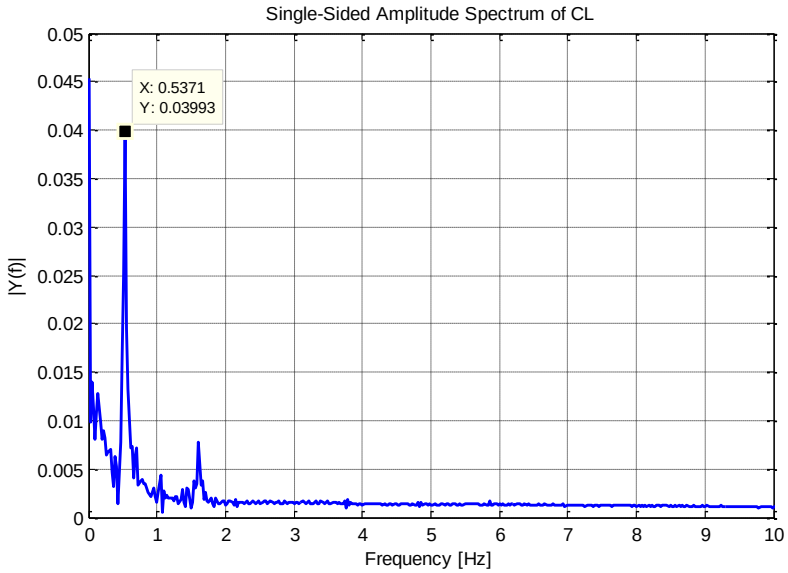

Figure 5. 13 Discrete Fourier transformation result of lift oscillation of flow around a FB3500-2250 flatback airfoil at Re = 1000 – VPM result

Comparisons of lift coeficients, drag coefficients and Strouhal numbers obtained from VPM and CFD analysis for FB3500-1750 and FB3500-2250 airfoils are presented in Table 5.1 and Table 5.2. It should be noted that drag coefficients given in Table 5.1 and Table 5.2 are due to pressure forces. Since the forces calculated with VPM is obtained by considering only pressure forces, drag coefficients due to viscous forces in CFD results are neglected.

Table 5. 1 Comparison of VPM and CFD Results for FB3500-1750 Flatback Airfoil at Re = 1000

Parameter	VPM Results	CFD Results
C_L (mean)	-0.0112	-0.0115
C_L (rms)	0.0259	0.0267
C_D (mean)	0.1508	0.1390
Strouhal Number	0.0940	0.1030

Table 5. 2 Comparison of VPM and CFD Results for FB3500-2250 Flatback Airfoil at Re = 1000

Parameter	VPM Results	CFD Results
C_L (mean)	-0.0221	-0.0189
C_L (rms)	0.0283	0.0296
C_D (mean)	0.1650	0.1430
Strouhal Number	0.1210	0.1320

Comparison of results shows that drag coefficients, lift coefficients and Strouhal numbers obtained from VPM and CFD analyses are well-matched. As can be explained before, the small difference between drag coefficient results is due to the difference between base pressures.

CHAPTER 6

CONCLUSION

6.1. Summary

In the present study, aerodynamic analysis of flatback airfoils are investigated by using vortex particle method, which is commonly used for simulation of two dimensional, incompressible, viscous flows. In the content of this thesis, vortex particle method code developed by Kaya [1] is improved by changing diffusion method. Previously, diffusion of vortex particles was modelled by means of Random Walk Method. In the present study, deterministic Particle Strength Exchange method is employed to solve diffusion equatiton. In addition, vorticity creation method, which provides the enforcement of boundary condition, is modified. Instead of generating particles at each time step as Kaya [1] did, number of particles in the flow domain is kept constant.

The validation and applicability of the improved algorithm is illustrated by solving several test cases which are flow past a flat plate, flow past a square cylinder and flow past a circular cylinder. After that, flow field around FB3500 series flatback airfoils at Reynolds number of 1000 are simulated by using the improved vortex particle method code. In order to compare results, laminar and unsteady CFD analyses are achieved. Comparisons show that reasonable flow features and physical quantities are obtained by present numerical simulations. VPM code provides fairly good results for laminar regime. Unlike RVM code which is developed by Kaya [1] and uses Random Walk Method to model diffusion, VPM simulation results do not

include noise. In additon, VPM algorithm has higher rate of convergenge and gives more stable results than RVM algorithm.

6.2. Recommendations for Future Works

In order to improve code, to be able to get more accurate results and to have more useful analysis tool, future works listed below could be implemented;

- The most time consuming part of the VPM code is velocity calculation subroutine. Fast algorithms could be used in this subroutine. For instance, poisson equation could be solved by using fast Fourier transform instead of direct method.
- In the present code, uniform grid size is employed. To decrease computational time, adaptive grid sizes could be used. For example, near the solid boundary, grid sizes could be much smaller than grid sizes of the rest of the domain.

REFERENCES

[1] H. Kaya, "Aerodynamic Analysis of Long-Span Bridge Cross-Sections Using Random Walk Method," Middle East Technical University, 2012.

[2] C. P. van Dam, "Blade Aerodynamics - Passive and Active Load Control for Wind Turbine Blades," Department of Mechanical & Aeronautical Engineering, University of California, 2009.

[3] T. Winnemöller and C. P. Van Dam, "Design and Numerical Optimization of Thick Airfoils Including Blunt Trailing Edges," *J. Aircr.*, vol. 44, no. 1, pp. 232–240, Jan. 2007.

[4] C. N. METZINGER, "Flatback Airfoils : An Experimental Evaluation of Aerodynamic Performance and Vortex Shedding Behavior," University of California, 2012.

[5] D. E. Berg and M. Barone, "Aerodynamic and Aeroacoustic Properties of a Flatback Airfoil (Will it Rumble or Whisper ?)," *AIAA Aerosp. Sci. Meet. Exhib. Wind.*, pp. 4–13, 2008.

[6] L. A. Barba, "Vortex Method for computing high-Reynolds number flows: Increased accuracy with a fully mesh-less formulation," California Institute of Technology, 2004.

[7] M. L. Ould-Salihi, G.-H. Cottet, and M. El Hamraoui, "Blending Finite-Difference and Vortex Methods for Incompressible Flow Computations," *SIAM J. Sci. Comput.*, vol. 22, no. 5, pp. 1655–1674, May 2000.

[8] F. M. Pepin, "Simulation of the flow past an impulsively started cylinder using a discrete vortex method," 1990.

[9] L. Rosenhead, “The formation of vortices from a surface of discontinuity,” in *Proceedings of the Royal Society of London*, 1931.

[10] A. J. Chorin, “Numerical study of slightly viscous flows.”

[11] A. Leonard, “Vortex methods for flow simulation,” *J. Comput. Phys.*, vol. 37, no. 3, pp. 289–335, 1980.

[12] T. Sarpkaya, “Computational Methods With Vortices—The 1988 Freeman Scholar Lecture,” *J. Fluids Eng.*, vol. 111, no. 1, pp. 5–52, Mar. 1989.

[13] C. REHBACH, “Numerical calculation of three-dimensional unsteady flows with vortex sheets,” in *16th Aerospace Sciences Meeting*, American Institute of Aeronautics and Astronautics, 1978.

[14] P. Degond and S. Mas-Gallic, “The Weighted Particle Method for Convection-Diffusion Equations Part 1 : The Case of an Isotropie Viscosity,” vol. 53, no. 188, pp. 485–507, 1989.

[15] P. D. Koumoutsakos, “Direct Numerical Simulations of Unsteady Separated Flows Using Vortex Methods,” California Institute of Technology, 1993.

[16] P. Ploumhans and G. . Winckelmans, “Vortex Methods for High-Resolution Simulations of Viscous Flow Past Bluff Bodies of General Geometry,” *J. Comput. Phys.*, vol. 165, no. 2, pp. 354–406, Dec. 2000.

[17] P. Ploumhans, G. S. Winckelmans, J. K. Salmon, a. Leonard, and M. S. Warren, “Vortex Methods for Direct Numerical Simulation of Three-Dimensional Bluff Body Flows: Application to the Sphere at Re=300, 500, and 1000,” *J. Comput. Phys.*, vol. 178, no. 2, pp. 427–463, May 2002.

[18] S. Yang, C. Cremona, Z. Zhou, and A. Chen, “Analysis of Reynolds number effects on bridge deck sections by the PSE method,” *Eur. J. Environ. Civ. Eng.*, vol. 15, no. 1, pp. 99–124, Jan. 2011.

[19] G.-H. Cottet and P. Koumoutsakos, *Vortex Methods: Theory and Practice*. Cambridge University Press, 2000.

[20] S. F. Hoerner, "Base Drag and Thick Trailing Edges," *J. Aeronaut. Sci. (Institute Aeronaut. Sci.*, vol. 17, no. 10, pp. 622–628, Oct. 1950.

[21] K. J. Standish and C. P. van Dam, "Aerodynamic Analysis of Blunt Trailing Edge Airfoils," *J. Sol. Energy Eng.*, vol. 125, no. 4, p. 479, 2003.

[22] T. Winnemöller and C. P. Van Dam, "Design and Numerical Optimization of Thick Airfoils Including Blunt Trailing Edges," *J. Aircr.*, vol. 44, no. 1, pp. 232–240, Jan. 2007.

[23] C. P. C. Van Dam, E. A. Mayda, D. D. Chao, and D. E. Berg, "Computational Design and Analysis of Flatback Airfoil Wind Tunnel Experiment," no. March, 2008.

[24] C. E. Mertes, "Dynamic Wake Studies of a Flatback Airfoil," The University of Wyoming, 2012.

[25] R. I. Lewis, *Vortex Element Methods for Fluid Dynamic Analysis of Engineering Systems*. Cambridge University Press, 1991.

[26] D. T. C. Porthouse, *Numerical Simulation of Aerofoil and Bluff Body Flows by Vortex Dynamics*. University of Newcastle upon Tyne, 1983.

[27] C. Norberg, "Flow Around a Circular Cylinder: Aspects of Fluctuating Lift," *J. Fluids Struct.*, vol. 15, no. 3–4, pp. 459–469, Apr. 2001.

[28] A. ROSHKO, "On the development of turbulent wakes from vortex streets," 1954.

[29] C. WIESELSBERGER, “Neuere Festellungen uKber die Gesetze des FluKssigkeits- und Luftwiderstandes,” *Phys. Zeitschrift*, vol. 22, pp. 321–328, 1921.

[30] B. N. Rajani, a. Kandasamy, and S. Majumdar, “Numerical simulation of laminar flow past a circular cylinder,” *Appl. Math. Model.*, vol. 33, no. 3, pp. 1228–1247, Mar. 2009.

[31] D.-H. Yoon, K.-S. Yang, and C.-B. Choi, “Flow past a square cylinder with an angle of incidence,” *Phys. Fluids*, vol. 22, no. 4, p. 043603, 2010.

[32] A. Sohankar and C. Norberg, “Numerical simulation of unsteady low-Reynolds number flow around rectangular cylinders at incidence,” vol. 71, pp. 189–201, 1997.

[33] A. Sohankar, C. Norberg, and L. Davidson, “Low-Reynolds-number flow around a square cylinder at incidence: study of blockage, onset of vortex shedding and outlet boundary condition,” *Int. J. Numer. Methods Fluids*, vol. 26, no. 1, pp. 39–56, 1998.

[34] A. Okajima, “Strouhal numbers of rectangular cylinders,” *J. Fluid Mech.*, vol. 123, no. -1, p. 379, Apr. 2006.